Cell Reports

Functional Oocytes Derived from Granulosa Cells

Graphical Abstract

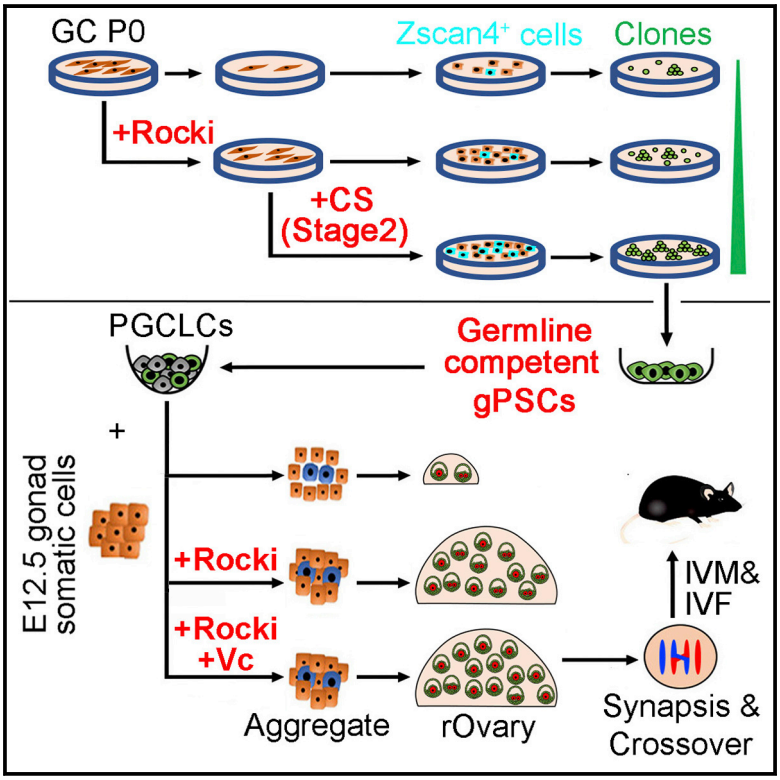

Highlights

- Granulosa cells can be reprogrammed to form oocytes by chemical reprogramming
- Rock inhibition and crotonic acid facilitate the chemical induction of gPSCs from GCs
- PGCLCs derived from gPSCs exhibit longer telomeres and high genomic stability

Authors

Chenglei Tian, Linlin Liu, Xiaoying Ye, ..., Huasong Wang, Dai Heng, Lin Liu

Correspondence

liulin@nankai.edu.cn

In Brief

Tian et al. report the successful generation of functional oocytes with genomic stability that produce fertile pups from adult-granulosa-cell-derived gPSCs through chemical reprogramming, which exhibits great potential for preserving fertility and restoring ovarian function.

Tian et al., 2019, Cell Reports *29*, 4256–4267
December 24, 2019
https://doi.org/10.1016/j.celrep.2019.11.080

CellPress

OPEN ACCESS
CellPress

Cell Reports
Report

Functional Oocytes Derived from Granulosa Cells

Chenglei Tian,[1,2] Linlin Liu,[1,2] Xiaoying Ye,[1,2] Haifeng Fu,[1,2] Xiaoyan Sheng,[1,2] Lingling Wang,[1,2] Huasong Wang,[1,2] Dai Heng,[1,2] and Lin Liu[1,2,3,4,*]

[1]State Key Laboratory of Medicinal Chemical Biology, Nankai University, 94 Weijin Road, Tianjin 300071, China
[2]Department of Cell Biology and Genetics, Nankai University, 94 Weijin Road, Tianjin 300071, China
[3]The Key Laboratory of Bioactive Materials Ministry of Education, College of Life Sciences, Nankai University, 94 Weijin Road, Tianjin 300071, China
[4]Lead Contact
*Correspondence: liulin@nankai.edu.cn
https://doi.org/10.1016/j.celrep.2019.11.080

SUMMARY

The generation of genomically stable and functional oocytes has great potential for preserving fertility and restoring ovarian function. It remains elusive whether functional oocytes can be generated from adult female somatic cells through reprogramming to germline-competent pluripotent stem cells (gPSCs) by chemical treatment alone. Here, we show that somatic granulosa cells isolated from adult mouse ovaries can be robustly induced to generate gPSCs by a purely chemical approach, with additional Rock inhibition and critical reprogramming facilitated by crotonic sodium or acid. These gPSCs acquired high germline competency and could consistently be directed to differentiate into primordial-germ-cell-like cells and form functional oocytes that produce fertile mice. Moreover, gPSCs promoted by crotonylation and the derived germ cells exhibited longer telomeres and high genomic stability like PGCs *in vivo*, providing additional evidence supporting the safety and effectiveness of chemical induction, which is particularly important for germ cells in genetic inheritance.

INTRODUCTION

Germ cells develop into mature oocytes that become competent in fertilization and produce live offspring, and they are essential for the propagation of all vertebrate species (Edson et al., 2009; Matzuk et al., 2002). Nevertheless, germ cells and follicle reserves are determined at birth, and the depletion of a finite germ cell reserve and the declining quality of oocytes with age or chemotherapy lead to reproductive or premature aging and associated diseases, including infertility (Findlay et al., 2015; Grive and Freiman, 2015; Nagaoka et al., 2012; Zhang and Liu, 2015). The generation of oocytes would hold great potential in preserving and restoring fertility. In addition, before the discovery of induced pluripotent stem cells (iPSCs), oocytes were the only source used for therapeutic cloning to generate somatic cell nuclear transfer (SCNT) embryonic stem cells (ESCs) for autologous regenerative medicine. Oocyte derivation has been pursued extensively using various approaches in the last decade or so, notably from ESCs and reported as early as 2003 (Hübner et al., 2003), and finally was achieved successfully from ESCs and iPSCs (Hayashi et al., 2012), showing great potential for clinical application (Gell and Clark, 2018).

Presumably, female cells are the appropriate source for generating oocytes by reprogramming. The accessible granulosa cells (GCs) are somatic cells that interact and evolve with oocyte development during folliculogenesis in the ovary and exhibit stem-cell-like properties (Coticchio et al., 2015; Edson et al., 2009; Hummitzsch et al., 2015; Matzuk et al., 2002). GCs are amenable to reprogramming to generate iPSCs by only two transcription factors, and they have been successfully used to clone animals (Mao et al., 2014; Polejaeva et al., 2000; Wakayama et al., 1998; Zuo et al., 2012). These factors prompted us to explore the potential of GCs in deriving oocytes via reprogramming and differentiation using a simple method without cell transfection.

Encouragingly, cellular reprogramming to pluripotent stem cells by small molecules alone, termed chemically induced pluripotent stem cells (CiPSCs), originally discovered by the Deng group, has been achieved in several laboratories (Cao et al., 2018; Fu et al., 2018; Long et al., 2015; Ye et al., 2016; Zhao et al., 2015, 2018). This approach avoids genetic manipulation, cell transfection, and ectopic expression of transcription factors for iPSCs and avoids embryo destruction for ESC derivation. Hence, CiPSCs provide an alternative source with greater potential in stem cell-based therapy. In published literature, CiPSCs induced mainly from fetal and neonatal fibroblasts with XY chromosomes or undefined sex are shown to possess germline competency. Germline transmission competence is well accepted as the high standard to evaluate naive pluripotency and is regarded as essential for induction of germ cells. Meanwhile, the strict genome fidelity required for germ cells inspired us to test reprograming of GCs by small molecules alone. However, it is unclear thus far whether adult female cells are able to generate germline-competent PSCs (gPSCs) by small molecules alone and whether CiPSCs can be directed to differentiate into germ cells and functional oocytes. We undertook experiments to test whether GCs isolated from adult mouse ovaries can be induced to gPSCs using a purely chemical approach and

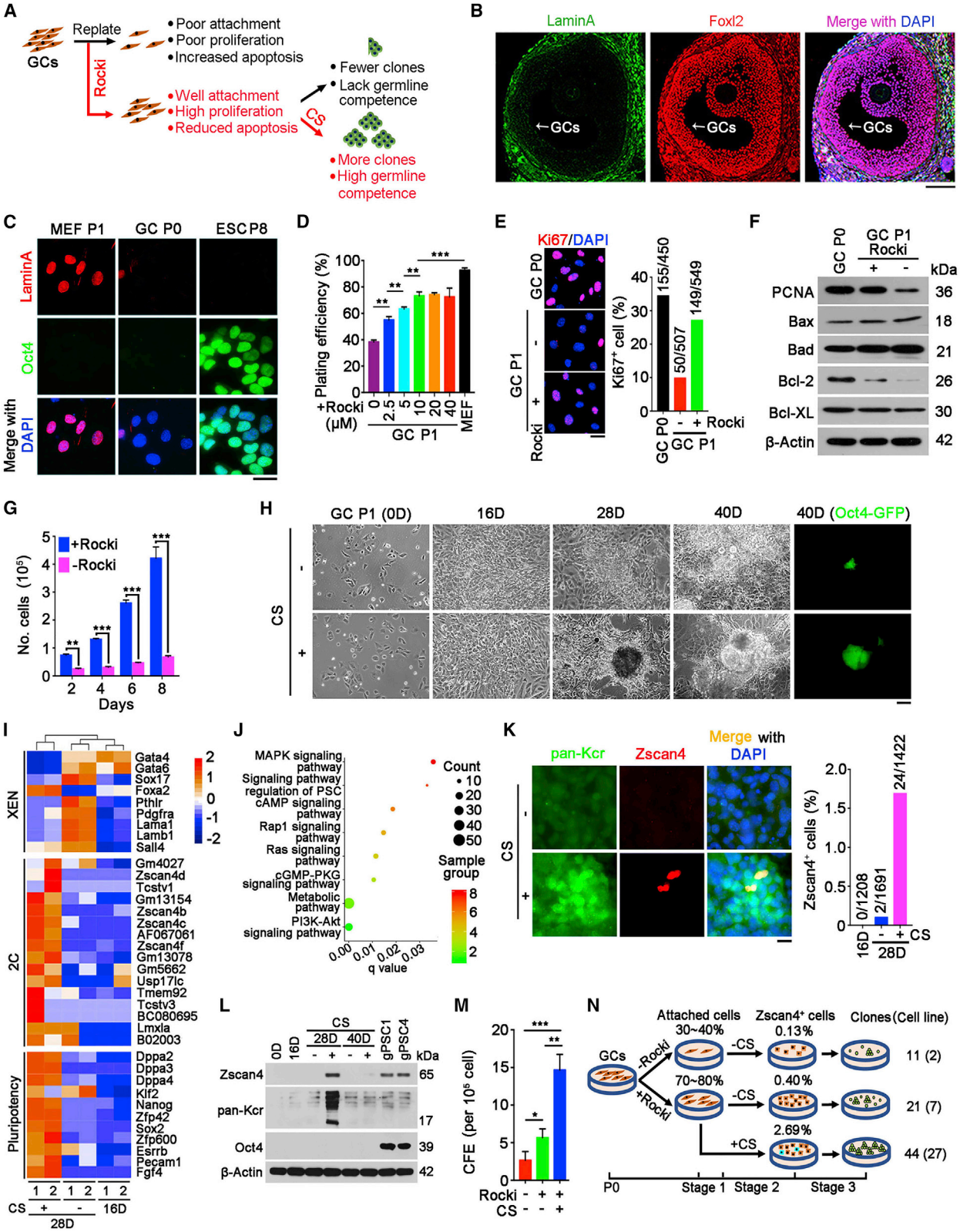

(legend on next page)

whether these gPSCs can be further induced to form oocytes with high genomic stability that produce fertile mice.

RESULTS

Optimization of Inducing Pluripotent Stem Cells from GCs (gPSCs) by a Purely Chemical Approach

We attempted to generate gPSCs based on the method described (Zhao et al., 2015) by testing additional small chemicals (Figure 1A). GCs were isolated from 6-week-old female Oct4-GFP mice (OG2 mice, C57BL6 X CBA). We compared the transcriptome of passage 0 (P0) GCs at primary culture for 7 days with that of mouse embryonic fibroblasts (MEFs) by RNA sequencing (RNA-seq) analysis. The transcription profile of GCs differed from that of MEFs (Figures S1A and S1B). In addition to higher expression of GC marker genes, the metabolic genes, especially those involved in the steroid metabolic process, were expressed at higher levels in GCs compared with MEFs (Figures S1C–S1E). By immunofluorescence, Foxl2-positive GCs of 6-week-old ovaries were negative for expression of nuclear envelope LaminA (Figure 1B), a marker for cell differentiation (Constantinescu et al., 2006). Moreover, immunofluorescence of *in vitro* cultured GCs verified that GCs only expressed less LaminA, like ESCs (Constantinescu et al., 2006) (Figure 1C; Figures S1F and S1G). In contrast, MEFs highly expressed LaminA, correlating with their fully differentiated state (Bru et al., 2008) (Figure 1C). Furthermore, RNA-seq comparison of MEFs, GCs, and extra-embryonic endoderm (XEN)-like cells revealed that GCs were more similar than MEFs to XEN-like cells regarding global transcriptome or expression of XEN marker genes (*Gata4*, *Lama1*, *Tinagl1*, etc.) (Figures S1H–S1J). These results suggested that GCs, as an accessible cell source, are closer to the XEN-like state, an intermediate stage toward CiPSCs (Zhao et al., 2015).

We attempted to induce GCs to PSCs (gPSCs) by taking advantage of a chemical reprogramming approach originally developed using MEFs (Zhao et al., 2015). The method requires three stages to completely induce CiPSCs via a XEN-like state, differing from the pathway of transcription factor-induced reprogramming (Zhao et al., 2015). However, GCs are deficient in proliferation and attachment in *in vitro* culture. By screening several chemicals in initial experiments, we found that Y27632, a Rock inhibitor (Rocki), improved the plating efficiency of GCs in a dose-dependent manner (Figure 1D). Compared with the control (Ctrl), adding 10 μM Rocki increased the number of Ki67-positive GCs (Figure 1E). Moreover, Rocki treatment elevated the expression of proliferating cell nuclear antigen (PCNA) and the anti-apoptosis protein Bcl-2 (Figure 1F), such that Rocki increased the number of GCs in culture (Figure 1G). Hence, Rocki treatment improved attachment, enhanced proliferation, and prevented apoptosis of GCs (Figure 1A).

Yet the efficiency in generating gPSCs from GCs by small molecules was still very low. We could only pick 21 clones from three repeated experiments and established 7 cell lines (Figure 1A). Furthermore, these gPSC lines showed limited competence to generate chimeras and failed to give rise to germline-competent offspring (Table S1). Recently, we found that crotonylation with crotonic acid (CA) or sodium (CS, crotonic acid added with 1 N NaOH to adjust the pH to approximately 7.0) at stage 2 of reprogramming activates 2-cell embryo (2C) genes, notably Zscan4, which improves induction efficiency (Fu et al., 2018). Thus, we tested and systematically compared whether CS can facilitate the generation of gPSCs from GCs. Consistently, CS significantly accelerated reprogramming processes and enhanced gPSC induction (Figure 1H). By RNA-seq analysis, the 2C genes,

Figure 1. Rock Inhibitor and Crotonic Sodium Facilitate the Induction of Pluripotent Stem Cells from Granulosa Cells (gPSCs) by aPurely Chemical Approach

(A) Schematic summary illustrating the strategy for deriving gPSCs by a purely chemical approach, and key improvements of this work (highlighted in red). Rocki, rock inhibitor, known as Y27632; CS, crotonic sodium (pH 7.0).

(B) Granulosa cells (GCs) in follicles of adult mouse ovaries express the GC marker Foxl2 (red) but no or minimal nuclear envelope LaminA (green) by immunofluorescence. Scale bar, 100 μm.

(C) GCs cultured *in vitro* rarely express LaminA, like ESCs, in contrast to female MEFs by immunofluorescence. Scale bar, 20 μm.

(D) Dose dependence of Rocki (0 to 40 μM) in improving efficiency of GC attachment at passage 1 (P1). Plating efficiency was measured by the number of attached cells divided by the number of plated cells. MEFs served as a control.

(E) Rocki treatment improves proliferation of GCs, as determined by immunofluorescence of Ki67. The ratio of $Ki67^+$ cells was measured by the number of $Ki67^+$ cells divided by the number of DAPI-stained cells. Scale bar, 20 μm.

(F) Rocki treatment elevates PCNA and Bcl-2, as determined by western blot. β-actin served as a loading control.

(G) Rocki treatment increases the number of GCs during culture at passage 1.

(H) CS added at stage 2 (16–28 days) during gPSC induction improves clonal formation. XEN-like cells were observed on day 16, and clones in CS-treated cells are larger and more compact than those without CS on day 28 and day 40. Scale bar, 100 μm.

(I) Heatmap showing that CS added at stage 2 elevates expression of 2C genes and pluripotent genes.

(J) Enriched pathways of differentially expressed genes (DEGs) by KEGG analysis of reprogrammed cells by day 28 after treatment with CS compared with treatment without CS.

(K and L) CS added at stage 2 increases Zscan4 expression, as determined by immunofluorescence (K) and western blot (L). β-actin served as a loading control. Scale bar, 20 μm.

(M) CS improves gPSC clone formation by colony formation efficiency (CFE) analysis. CFE was estimated by the number of Oct4-GFP-positive clones on day 40 based on the total number of cells plated (10^5 cells).

(N) Summary of gPSC induction facilitated by Rocki and CS. The percentage of $Zscan4^+$ cells was obtained by FACS. Stage 1, 0–16 days; stage 2, 16–28 days; stage 3, 28–40 days.

Data are shown as mean ± SEM (n = 3). *$p < 0.05$, **$p < 0.01$, ***$p < 0.001$.

See also Figure S1 and Table S1.

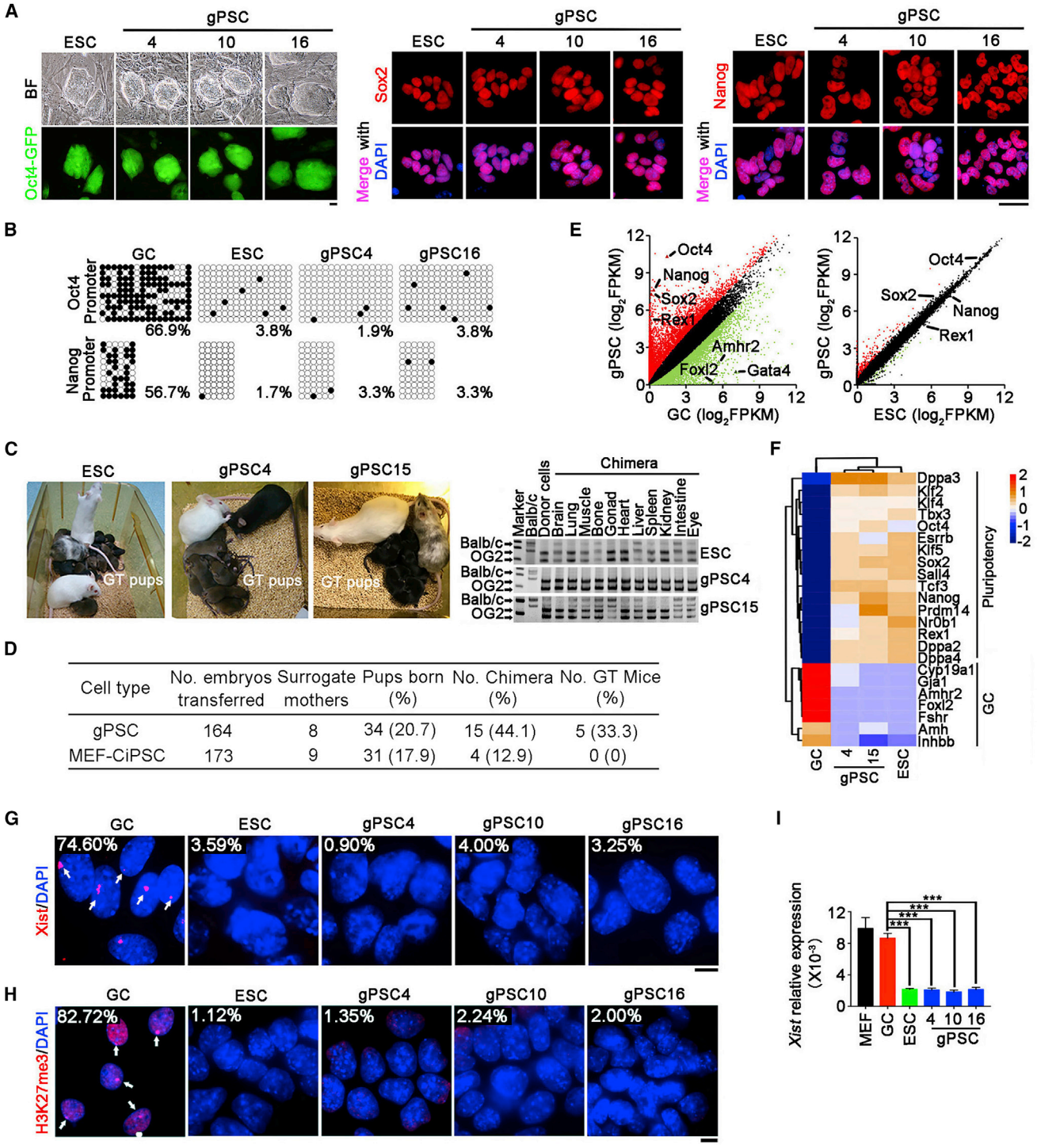

Cell type	No. embryos transferred	Surrogate mothers	Pups born (%)	No. Chimera (%)	No. GT Mice (%)
gPSC	164	8	34 (20.7)	15 (44.1)	5 (33.3)
MEF-CiPSC	173	9	31 (17.9)	4 (12.9)	0 (0)

Figure 2. gPSCs Acquire High Germline Competence

(A) Morphology and expression of pluripotency markers of gPSCs and female ESCs. Scale bar, 30 μm.

(B) Low level of methylation at *Oct4* and *Nanog* promoter regions in gPSCs. White dots indicate unmethylated loci, and dark spots indicate methylated loci.

(C) Germline competency of gPSCs and female ESCs by injection into 4- to 8-cell embryos and genotyping by D12Mit136 microsatellite assay (right panel). Albino BALB/c mice served as embryo donors, and pseudo-pregnant albino Kunming mice served as surrogate mothers.

(D) Summary of chimeras and germline transmission (GT) pups by injection into 4- to 8-cell embryos of gPSCs and female MEF-CiPSCs.

(E) Scatterplots of genome-wide transcription. Parallel diagonal lines indicate the two-fold threshold in expression difference ($p < 0.05$).

(legend continued on next page)

such as *Zscan4*, *Tcstv1*, and *Tcstv3*, and pluripotency genes, such as *Dppa3*, *Klf2*, and *Nanog*, were expressed at higher levels and XEN genes, including *Gata4*, *Gata6*, and *Sox17*, were expressed at lower levels by CS than Ctrls without CS (Figure 1I). Kyoto Encyclopedia of Genes and Genomes (KEGG) database analysis showed that the addition of CS regulated the expression of genes related to pluripotency signaling pathways, such as mitogen-activated protein kinase (MAPK), regulation of PSCs, and phosphatidylinositol 3-kinase (PI3K)-Akt signaling (Figure 1J). CS promoted global crotonylation and activated Zscan4, as determined by immunofluorescence and western blot assay (Figures 1K and 1L). Rocki treatment increased Oct4-GFP clonal formation, and the combination of Rocki and CS dramatically increased the number of Oct4-GFP clones by about six-fold, such that 27 cell lines were successfully established from 44 clones picked (Figures 1M and 1N). These data indicated that a XEN-like state tends to activate 2C genes toward a pluripotent state enhanced by CS-induced histone crotonylation (Figures 1A and 1N).

Altogether, the addition of CS at stage 2 is critical for promoting the generation of CiPSCs by activating 2C genes, particularly Zscan4, during chemical induction.

gPSCs Facilitated by Crotonylation Acquire High Germline Competence

Because gPSCs derived from GCs by CS were the first definite adult female CiPSC lines, we further tested their pluripotency and germline competence. gPSCs generated by CS were similar to female ESCs in morphology and expression of pluripotent markers, such as Oct4-GFP, Sox2, and Nanog (Figure 2A; Figures S2A and S2B). The methylation level of *Oct4* and *Nanog* promoter regions in ESCs and gPSCs was very low (less than 4%), whereas these regions in GCs were hypermethylated (66.9% in *Oct4* promoter and 56.7% in *Nanog* promoter) (Figure 2B). More importantly, unlike female MEF-CiPSC lines (from the same background of OG2 mice), the gPSC lines generated under the same experimental conditions by treatment with CS exhibited a high capacity to generate chimeras with germline competence (Figures 1A, 2C, and 2D; Table S1). Six cell lines (gPSC2, gPSC4, gPSC10, gPSC11, gPSC15, and gPSC16) generated by adding CS at stage 2 during reprogramming were randomly chosen to test their pluripotency by some standard methods, including pluripotency marker gene expression by qPCR, immunofluorescence and/or western blot, chimera production, differentiation potential by teratoma formation or embryoid body (EB) formation tests, and RNA-seq or exome sequencing (exome-seq) analysis. The gPSC lines were tested for their abilities in chimera production, and two of them (gPSC4 and gPSC15) produced germline transmission offspring (Table S1). To understand the underlying molecular changes in the gPSCs induced from GCs, we performed RNA-seq analysis of those cell lines compared with GCs and ESCs. The genome-wide gene expression profile differed between gPSCs and GCs but was similar between gPSCs and ESCs (Figure 2E). In addition, signaling pathways that regulate pluripotency, such as Lif, Bmp4, and Wnt pathways, became more activated in gPSCs compared with GCs (Figure S2C). Like ESCs, gPSCs highly expressed marker genes for PSCs, such as *Oct4*, *Sox2*, *Nanog*, and *Rex1*, and only minimally expressed GC-specific genes, such as *Foxl2*, *Gata4*, and *Amhr2* (Figures 2E and 2F). X chromosome activation is another important indicator of full reprogramming in female iPSCs (Pasque et al., 2014). As expected, the inactivated X chromosome in GCs became reactivated in gPSCs through chemical reprogramming, resembling female ESCs (Figures 2G–2I).

In addition, gPSCs demonstrated differentiation capacity, like ESCs, as determined by EB formation assay *in vitro*, and were able to differentiate into three embryonic germ layers: ectoderm (βIII-tubulin-positive cells), mesoderm (smooth muscle actin [SMA]-positive cells), and endoderm (α-fetoprotein [AFP]-positive cells) (Figure S2D). Similar to ESCs, gPSCs can generate ectoderm, mesoderm, and endoderm, as determined by teratoma formation assay (Figure S2E). Immunofluorescence assays further showed that teratomas derived from ESCs or gPSCs expressed molecular markers representative of three germ layers, including Nestin (ectoderm), SMA (mesoderm), and AFP (endoderm) (Figure S2F). Therefore, GCs were successfully induced into gPSCs that exhibit pluripotency and differentiation potential like ESCs, along with X chromosome activation, and possess high germline competence.

Optimization for Folliculogenesis in Reconstituted Ovaries (rOvaries) from gPSCs

We improved upon a previously published method for inducing meiosis and oocyte growth by aggregation of primordial germ cells (PGCs) or PGC-like cells (PGCLCs) with fetal embryonic day (E) 12.5 somatic cells and mainly pre-GCs followed by kidney capsule transplantation (Qing et al., 2008; Shen et al., 2006), instead of the ovarian bursa transplantation method, which is more technically challenging. Initially, we employed the aggregation of somatic cells and pre-GCs with PGCs isolated from E12.5 gonad to form rOvaries for meiosis induction and folliculogenesis (Matoba and Ogura, 2011; Zeng et al., 2017). In the absence of phytohemagglutinin (PHA), 10 μM Rocki (Y27632) promoted the aggregation of PGCs with somatic cells to form rOvaries (Figure 3A). Aggregates in MF10 (M199 plus

(F) Heatmap highlighting the downregulation of GC marker genes such as *Foxl2*, *Amhr*, and *Fshr* and upregulation of pluripotent genes such as *Oct4*, *Dppa3*, *Klf2*, and *Esrrb* in gPSCs compared with GCs. ESCs served as control.

(G) *Xist* RNA FISH merged with DAPI analyzed for the status of X chromosome activation in gPSCs. The white arrow indicates *Xist*-positive cells. The proportion of *Xist*-positive cells is shown at the top in white. Scale bar, 5 μm.

(H) Immunofluorescence of H3K27me3 in gPSCs. White arrows indicate X chromosome inactivation. The proportion of X chromosome-inactivated cells is shown at the top in white. Scale bar, 5 μm.

(I) Lower expression level of *Xist* in gPSCs and female ESCs compared with GCs and MEFs by quantitative real-time PCR analysis. Data are shown as mean ± SEM (n = 3). ***$p < 0.001$.

See also Figures S1–S4 and Table S1.

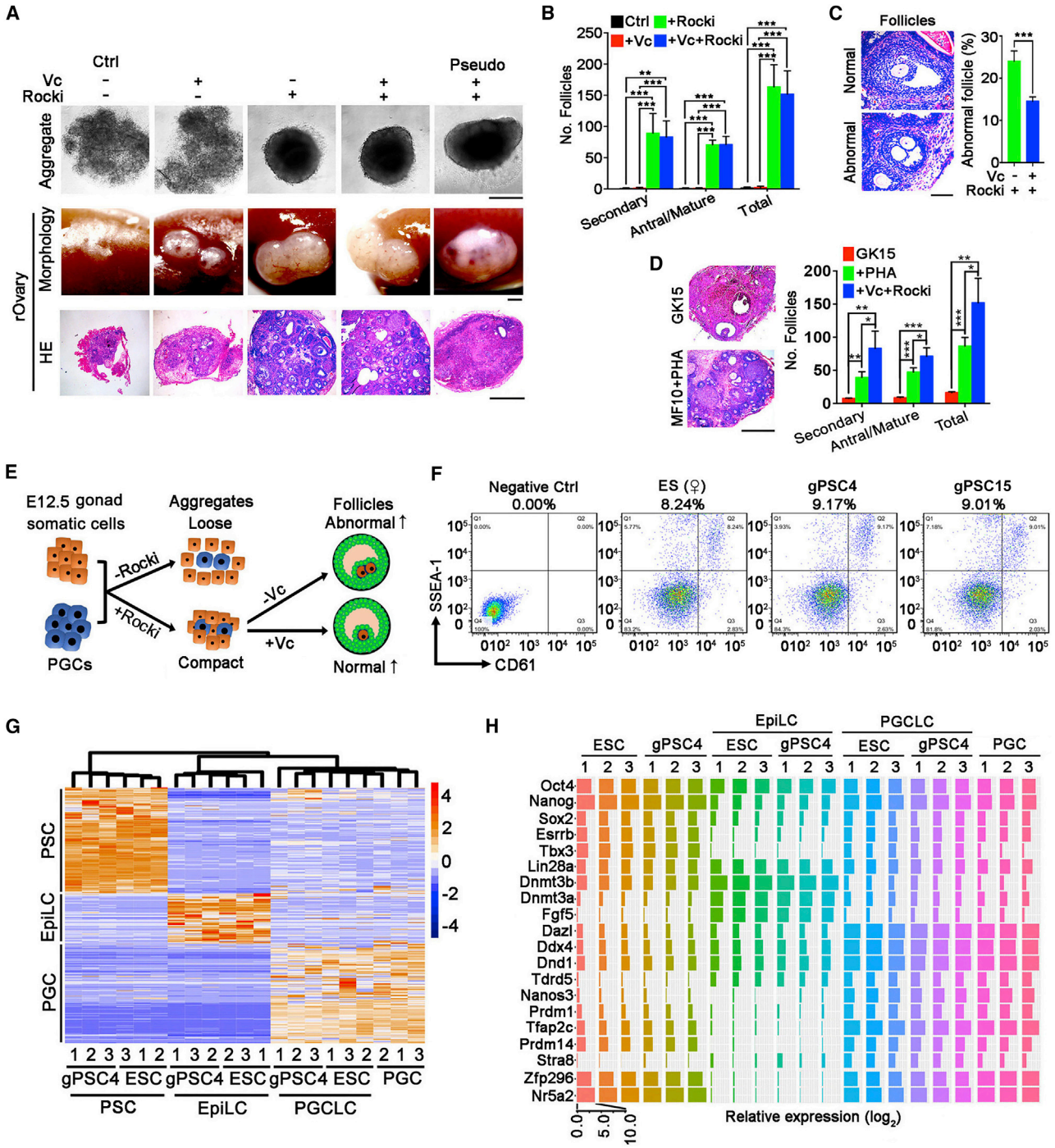

Figure 3. Improving Folliculogenesis in Reconstituted Ovaries (rOvaries) from gPSCs

(A) Rocki treatment promotes folliculogenesis of PGCs aggregated with E12.5 gonad somatic cells. Upper panel, morphology of aggregates; middle panel, morphology of rOvaries; lower panel, H&E staining. Pseudo indicates aggregated E12.5 gonad somatic cells only (without PGCs), and no follicles are observed in pseudo-rOvaries. Scale bar, 1 mm.

(B) Follicle count of rOvaries at 28 days following transplantation into the kidney capsule (n = 4).

(C) Vc improves the quality of follicles in rOvaries. Abnormal follicles have more than one oocyte in a follicle. Scale bar, 200 μm.

(D) H&E staining and follicle count of rOvaries formed from aggregates in GK15 medium or MF10 + PHA following transplantation into the kidney capsule. Scale bar, 1 mm. Right panel, comparison of the number of follicles formed from aggregates by treatment with three conditions (n = 4).

(E) Schematic diagram illustrating that Rocki treatment promotes the formation of aggregates and Vc enhances the quality of follicles in rOvaries.

(legend continued on next page)

10% fetal bovine serum [FBS]) with Rocki became more compact after aggregation for one day, and the resulting rOvaries were larger than Ctrls after transplantation to the kidney capsule for 28 days (Figure 3A). Furthermore, Rocki treatment increased the number of follicles developed in rOvaries (Figures 3A and 3B). As a negative Ctrl, pseudo-aggregates were formed from E12.5 gonad somatic cells alone without PGCs, but no follicles were found in the pseudo-aggregates after transplantation into the kidney capsule (Figure 3A). To test the purity of E12.5 gonad somatic cells, we collected those cells by stage-specific embryonic antigen-1 (SSEA1) magnetic-activated cell sorting (MACS), followed by fluorescence-activated cell sorting (FACS) using markers for PGCLCs, SSEA1, and CD61. No double-positive cells were observed in SSEA1-MACS-negative cells, indicating that the E12.5 gonad somatic cells did not contain PGCs.

In addition, we improved the quality of folliculogenesis in the rOvaries. Ascorbic acid (vitamin C [Vc]) as a direct regulator of Tet activity, enhances meiosis through epigenetic modification (Suzuki et al., 2016; Yamaguchi et al., 2012). The addition of 50 μg/mL of Vc during aggregation facilitated the correct assembly of follicles and reduced the number of abnormal follicles (more than one oocyte in a follicle) (Figure 3C). Moreover, compared with previous media used for aggregation, such as GMEM plus 15% knockout serum replacement (KSR) (GK15) (Hayashi and Saitou, 2013) or MF10 plus PHA (MF10 + PHA) (Qing et al., 2008), our aggregation method using MF10 in combination with Rocki and Vc significantly increased the number of high-quality follicles per rOvary following kidney capsule transplantation (Figure 3D). The refined culture and aggregation conditions supported the aggregation and follicle formation of rOvaries (Figure 3E) and were used for subsequent experiments.

We induced PGCLCs from gPSCs by following a previously described protocol (Hayashi et al., 2012; Hayashi and Saitou, 2013). gPSCs were efficiently induced into epiblast-like cells (EpiLCs) and further into PGCLCs (Figure S2G), with an efficiency similar to that of ESCs, as determined by FACS (Figure 3F). To understand the molecular changes in the PGCLCs derived from gPSCs, we performed RNA-seq analysis of these cells and compared them with E12.5 PGCs *in vivo*. ESCs and gPSCs, EpiLCs, and PGCLCs were readily distinguishable at the transcriptome level and by their own specific markers (Zhou et al., 2016) (Figure 3G). PGCLCs differentiated from female ESCs or gPSCs exhibited transcriptome profiles similar to those of PGCs *in vivo* and expressed PGC-specific genes (Zhou et al., 2016) (Figure 3H). Genes commonly associated with germ cells, such as *Dazl* and *Ddx4*/*Vasa*, were upregulated in PGCLCs. *Prdm1* (also called *Blimp1*), *Prdm14*, and *Tfap2c* were highly expressed in PGCLCs, like PGCs, but distinct from EpiLCs. The three genes are key in germ cell specification, and their combinations can induce PGCLCs (Chen et al., 2018; Magnúsdóttir et al., 2013; Magnúsdóttir and Surani, 2014; Nakaki et al., 2013; Ohinata et al., 2009; Pastor et al., 2018). Two recently identified PGCLC marker genes, *Nr5a2* and *Zfp296*, which play an important role in PGC specification (Hackett et al., 2018), were expressed at similarly high levels between PGCs and PGCLCs from gPSCs and were downregulated in EpiLCs (Figure 3H).

By using the optimized method for aggregation, gPSC-derived PGCLCs aggregated with E12.5 gonad somatic cells and formed condensed spheres, resembling those of ESC-derived PGCLCs and E12.5 PGCs (Figure S2H). The aggregates developed into rOvaries 28 days after transplantation into the kidney capsule (Figure S2H). We analyzed the function of rOvaries by determining the endocrine activity and measured the serum levels of follicle-stimulating hormone (FSH), estradiol (E2), and anti-Mullerian hormone (AMH) in host non-obese diabetic-severe combined immunodeficiency (NOD-SCID) mice. Compared with bilateral oophorectomy (OE) without rOvary grafts as negative Ctrls, serum FSH levels were reduced and levels of E2 and AMH were elevated in recipients with rOvary grafts (Figure S2I), indicating that PGCLCs originating from GCs develop into functional rOvaries that have the capacity for hormone production and secretion.

Induction of Meiosis and Fertile Pups from gPSCs

To determine the normality of meiosis progression in PGCLCs derived from gPSCs, we analyzed homologous chromosome pairing and synapsis by immunofluorescence microscopy of appropriate SCP1/3 elements and recombination by MLH1, key events that take place at meiosis prophase I (Handel et al., 2014). Transplantation of aggregates treated with 3 μM retinoic acid (RA) for one day into the kidney capsule with bilateral OE for 5 days allowed PGCs or PGCLCs to enter meiosis, similar to meiocytes in E16.5–E17.5 female gonads. E12.5 gonad somatic cells facilitate induction of meiosis from PGCs or PGCLCs. Purity of E12.5 gonad somatic cells sorted by MACS using SSEA1 antibody was validated by FACS using SSEA1/CD61 antibodies such that more than 99.99% somatic cells were SSEA1/CD61 negative, indicating absent or minimal contamination of PGCs, if any, in the sorted E12.5 gonad somatic cells (Figure 4A). PGCs aggregated with E12.5 gonad somatic cells differentiated into SCP3-positive meiocytes, in contrast to the pseudo-aggregates formed from only E12.5 gonad somatic cells that showed no SCP3 meiocytes as a negative Ctrl (Figure 4B).

SCP1/3 formed the axial elements of the synaptonemal complex completed at the pachytene stage, and an appropriate number of synaptonemal complex elements at the pachytene stage was found in meiocytes of gPSC-PGCLCs, similar to that of ESC-PGCLCs and E12.5 PGCs (Figure 4C). MLH1 foci normally appeared at the crossover sites, and the number of MLH1 foci did not differ among meiocytes of PGCs and PGCLCs

(F) Similar efficient induction of PGCLCs from gPSCs and ESCs by FACS. The SSEA1 and CD61 double-positive cells are PGCLCs; samples lacking the antibody served as a negative control.
(G) Heatmap highlighting the expression pattern of marker genes for PSCs, EpiLCs, and PGCLCs compared with E12.5 PGCs by RNA-seq.
(H) Key marker gene expression of PSCs, EpiLCs, PGCLCs, and PGCs by RNA-seq.
Data are shown as mean ± SEM. *$p < 0.05$, **$p < 0.01$, ***$p < 0.001$.
See also Figures S2–S4.

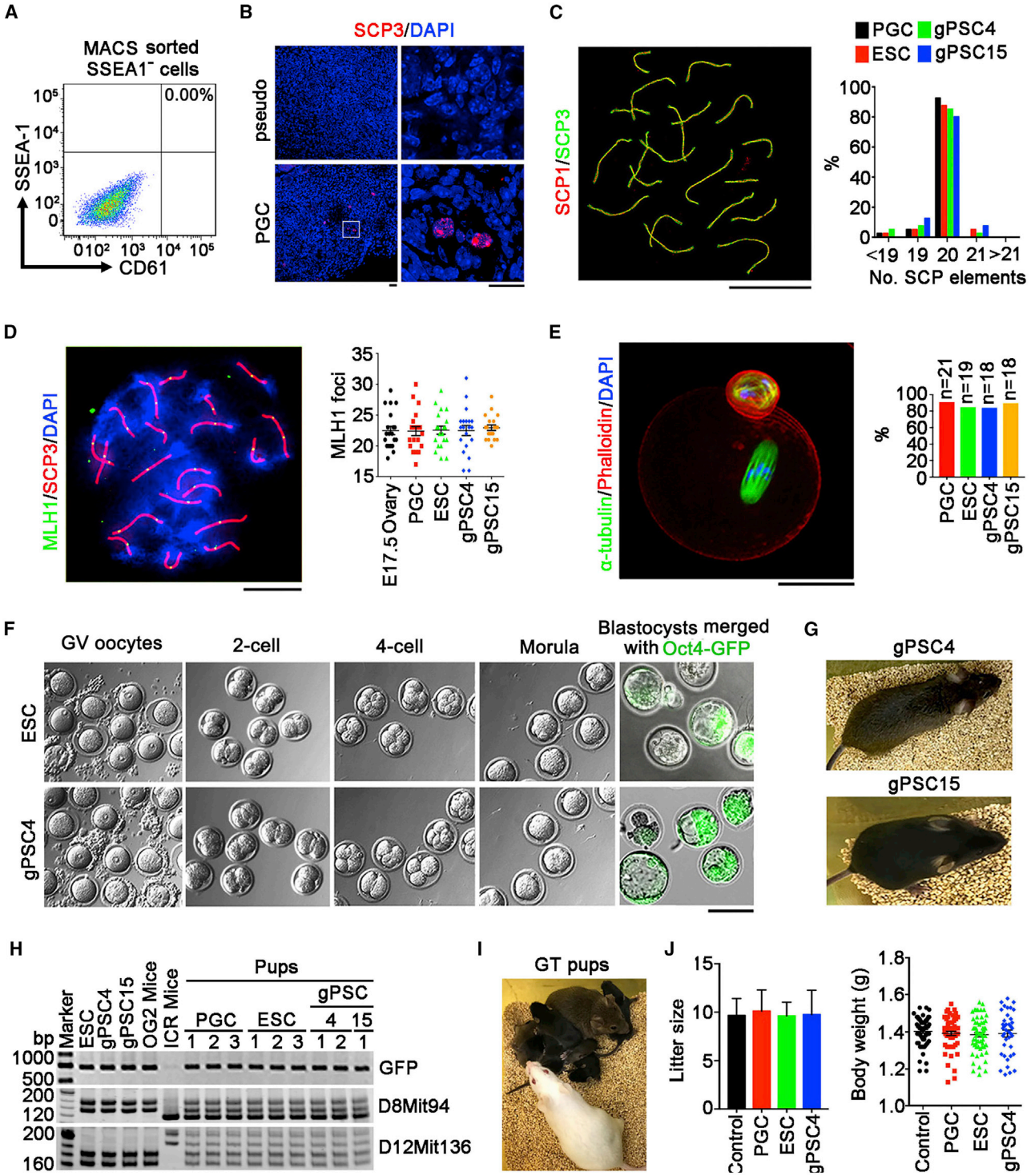

Figure 4. Production of Fertile Pups from Oocytes of gPSCs

(A) FACS analysis conformed absent SSEA1^{+}CD61^{+} cells in the SSEA1^{-} cells sorted by MACS.

(B) Pachytene spread was not observed in pseudo-rOvaries but was observed in PGC-rOvaries by immunofluorescence of SCP3 in the paraffin sections. Scale bar, 20 μm.

(C) Percentage of the normal number of synaptonemal complexes in gPSC- and ESC-derived meiocytes 5 days following transplantation of the aggregates based on pachytene spread (n = 40) (image shown was captured by super-high-resolution microscopy [SIM]). Scale bar, 5 μm.

(D) Statistics of MLH1 foci per cell at the pachytene stage in gPSC- and ESC-derived meiocytes. Scale bar, 5 μm.

(legend continued on next page)

differentiated from ESCs or gPSCs (Figure 4D). Furthermore, these PGCLC-derived germinal vesicle (GV) oocytes could mature to metaphase II (MII) oocytes with correct spindle assembly and chromosome alignment (Figure 4E). The proportion of MII oocytes with normal spindles developed from gPSC-PGCLCs did not differ from that of ESC-PGCLCs or E12.5 PGCs (Figure 4E). Hence, PGCLCs derived from gPSCs underwent normal meiosis and formed oocytes.

To test whether oocytes originated from GCs are capable of producing fertile pups, we mechanically dissected oocytes from follicles of the rOvaries and performed *in vitro* maturation (IVM) and *in vitro* fertilization (IVF). PGCLC-derived oocytes were able to reach the MII stage, be fertilized, and then be cleaved into 2-cell embryos and developed to blastocysts (Figure 4F). The IVM efficiency of GV oocytes was about 40%–50%, and cleavage to the 2C stage after IVF was approximately 20%–40%. Some 2Cs from PGCLCs were allowed to develop further to blastocysts. These blastocysts expressed Oct4-GFP (Figure 4F), and the developmental rate of cleaved embryos into blastocysts was 46%. Excitingly, four live pups were obtained following the transfer of 134 2Cs and one pup was obtained following the transfer of 37 blastocysts. The offspring from E12.5 PGCs and PGCLCs bore GFP transgenes and exhibited microsatellite markers of OG2 mice and ICR mice that contributed sperm (Figures 4G and 4H). Four mice survived, grew healthily to adulthood, and manifested normal fertility, as evidenced by giving birth to pups after mating with male albino ICR mice (Figure 4I). Litter size (approximately 10) and body weight of the offspring from gPSC-PGCLC-derived mice did not differ from those of natural breeding mice and of E12.5 PGC-derived mice (Figure 4J).

Telomere Reprogramming and Genomic Stability of gPSCs and Their Derived Germ Cells Originated from GCs

Genomic stability is particularly important for germ cells because of their unique roles in genetic inheritance. Telomeres protect chromosome ends and genomic stability, and they are maintained primarily by telomerase (Blackburn et al., 2015). gPSCs showed higher telomerase activity, as determined by telomeric repeat amplification protocol (TRAP) assay and ELISA and corroborated with higher expression levels of telomerase genes *Tert* and *Terc*, like ESCs, in comparison with GCs (Figures S3A–S3C). Moreover, telomeres lengthened in the formed gPSCs as estimated by the telomere/single-copy gene (T/S) ratio by quantitative real-time PCR assay and telomere restriction fragment (TRF) analysis and validated by telomere quantitative fluorescence *in situ* hybridization (Q-FISH) (Figures S3D–S3F). These data show that telomeres of GCs are rejuvenated in the formed gPSCs.

Because telomeres are elongated in gPSCs, we also measured telomere length in PGCLCs differentiated from gPSCs. PGCLCs induced from gPSCs or ESCs had longer telomeres than did E12.5 PGCs, as determined by both quantitative real-time PCR and telomere flow fluorescence *in situ* hybridization (Flow-FISH) assay (Figures S3G and S3H). The gPSCs/ESCs, EpiLCs, and PGCLCs exhibited similarly elongated telomeres (Figures S3G and S3H). Telomere Q-FISH also showed longer telomeres in gPSCs or ESC-derived pachytene meiocytes than those of pachytene meiocytes obtained from E17.5 gonad (Figure S3I). Hence, telomeres rejuvenated in PGCLCs and meiocytes originated from GCs (Figure S3J).

Furthermore, we examined genomic stability by exome-seq analysis of gPSC lines and compared them with the high-quality ESC line, OG4-ESCs. To perform molecular assessment of the potential mutation landscape across the OG4-ESC and gPSC samples, we called variants of gPSC lines, compared them with the parental GCs, and then filtered variants by a previously reported method (Gore et al., 2011). The signature and fraction of gene mutations appeared to be similar in OG4-ESC and three gPSC lines (Figures S4A and S4B). Moreover, the somatic mutations by a thorough single-nucleotide analysis in the coding sequence (CDS) region in three gPSC lines were lower than those of OG4-ESCs (less than 10) (Figures S4C and S4G). Although the total number of insertions or deletions (indels) in CDS in gPSC lines was slightly higher than that of OG4-ESCs, most of them represented non-frameshift mutations that may have no effect on gene expression (Figures S4C and S4G). These data indicate that high-quality gPSCs induced from GCs by small molecules alone maintain genomic stability.

Evaluating somatic mutations by a thorough single-nucleotide analysis of how the genome changes from biopsy to egg is imperative for regenerating germline cells *ex vivo* to progress from bench to bedside (Gell and Clark, 2018). To assess genomic stability during PGCLC induction, we performed exome-seq comparisons between E12.5 PGCs and gPSC4/15-PGCLCs and between wild-type (natural) GV oocytes and GV oocytes derived from gPSC pups. Frequencies of somatic mutations and indels in CDS of PGCLCs were very low and were not significantly different from those of PGCs *in vivo* (Figure S4D), suggesting that the induction of PGCLCs from gPSCs does not alter genome stability. Frequencies of somatic mutations and indels in CDS of GV oocytes generated from gPSC-derived pups also were very low and did not differ from those of GV oocytes derived *in vivo* from wild-type/natural mice (Figure S4E). No significant difference was observed in the frequency of somatic mutations and indels of CDS among gPSCs, gPSC-PGCLCs, and gPSC-GV

(E) Analysis of the frequency of normal MII oocytes with intact spindles and correct chromosome alignment from gPSC- and ESC-derived oocytes. Scale bar, 50 μm.
(F) GV oocytes isolated from gPSC and ESC rOvaries, and embryo development after IVM and IVF. Scale bar, 100 μm.
(G) Healthy adult mice generated from gPSC-PGCLC-derived oocytes by IVM and IVF.
(H) Genotyping analysis of the pups by GFP and microsatellite primers D8mit94 and D12Mit136. DNA was isolated from tail tip tissues.
(I) Germline competency of gPSC4-PGCLC-derived mice by mating with albino ICR mice.
(J) Similar litter size and body weight of pups produced from PGCs, ESCs, and gPSCs in comparison with those of wild-type/natural mice served as a control. See also Figures S2–S4.

oocytes (Figures S4F and S4G). These data demonstrated that PGCLCs differentiated from gPSCs and the resulting GV oocytes exhibited genome stability like natural PGCs and GV oocytes.

DISCUSSION

We successfully generated functional oocytes with genomic stability that produce fertile pups from adult GCs through a chemical reprogramming approach and PGCLC induction. Nevertheless, at least three obstacles were encountered and resolved during the process. First, although GCs show stem cell properties, they are deficient in cell proliferation and attachment when cultured *in vitro*. By testing various compounds, we found that treatment with a Rocki effectively enhanced the attachment of GCs to the culture dish, prevented apoptosis, and promoted proliferation, factors that are important for obtaining a sufficient number of primitive GCs for reprogramming.

In addition, we employed a chemical reprogramming approach (Zhao et al., 2015), for inducing PSCs from GCs. Unexpectedly, despite their stem-cell-like properties, GCs isolated from adult mouse ovaries were extremely inefficient in forming CiPSCs using the same CiPSC approach, and the formed CiPSCs do not have germline competence. These data also show that each cell type could differ markedly in abilities of CiPSC induction and germline competence. The method used for inducing germline-competent CiPSCs from MEFs may require slight but critical modifications if applied to other cell types. In addition, MEFs can be good starting sources for research, but the inaccessibility of fetal tissues limits the usefulness of fetal fibroblasts in inducing CiPSCs for feasible regenerative medicine in adults. We find that crotonic acid/CS-mediated crotonylation, which activates 2C genes, including Zscan4, during induction (Fu et al., 2018), is critical for successful derivation of gPSCs from adult GCs. Single-cell analysis also revealed the critical role of activating 2C genes and Zscan4 in improving CiPSC induction (Zhao et al., 2018). These results corroborate previous findings that activation of Zscan4 during induction by Yamanaka factors reduces telomere and genome damage and improves iPSC induction and quality (Hirata et al., 2012; Jiang et al., 2013).

Third, we improved the induction of meiosis and folliculogenesis from aggregates of PGCLCs with somatic cells by kidney capsule transplantation (Qing et al., 2008; Shen et al., 2006). We showed that Vc and Rocki treatment also were important for effective aggregation, induction of meiosis, and oocyte and follicle development of PGCLCs aggregated with fetal gonad somatic cells, including pre-GCs.

Our data demonstrated that CiPSCs are capable of producing germ cells and oocytes. Importantly, gPSCs induced by a purely chemical approach maintain genome integrity. Germ cells and oocytes rejuvenated from GCs without genetic modifications and transfection maintain high genomic stability, and longer telomeres and the offspring show normal fertility. Altogether, with an established optimized chemical reprograming approach, adult GCs are suitable sources for deriving PSCs and functional oocytes. Moreover, the derived gPSCs show high germline competence and genome integrity and thus are ideal for rejuvenation of functional oocytes for preserving or restoring fertility, as well as for regenerative medicine. Recently, PGCLCs have been successfully induced from human ESCs (hESCs) or human iPSCs (hiPSCs) (Irie and Surani, 2017; Irie et al., 2015; Sasaki et al., 2015), and encouragingly, these hESC- or hiPSC-derived PGCLCs can differentiate into oogonia (Yamashiro et al., 2018). In human fertility clinics, retrieved oocytes are used for IVF, but the GCs accompanied by oocytes are often discarded as by-products. Using GCs to produce oocytes via chemical reprogramming not only has potential for treating infertility but also may have implications in preserving fertility and endocrine function.

STAR★METHODS

Detailed methods are provided in the online version of this paper and include the following:

- KEY RESOURCES TABLE
- LEAD CONTACT AND MATERIALS AVAILABILITY
- EXPERIMENTAL MODEL AND SUBJECT DETAILS
  - Mice
  - Isolated and Primary Cultured Mouse Embryonic Fibroblasts
  - Mouse ESC Lines
  - Isolated and Primary Cultured Granulosa Cells
- METHOD DETAILS
  - Proliferation Curve of Granulosa Cells
  - Induction of gPSCs from Granulosa Cells
  - Induction of PGC-like Cells
  - Induction of Meiosis and Folliculogenesis
  - Magnetic Activated Cell Sorting
  - Kidney Capsule Transplantation
  - *In Vitro* Maturation and *In Vitro* Fertilization
  - Embryoid Body Formation Assay
  - Teratoma Formation Assay
  - Production of Chimeras and Genotyping
  - Follicle Count
  - Immunofluorescence Microscopy
  - Fluorescence Microscopy of Teratoma or Tissue Sections
  - Fluorescence Microscopy of Meiocyte Spreads
  - Immunofluorescence Microscopy of Spindle
  - Hormone Assays
  - Gene Expression Analysis by Real-Time qPCR
  - Western Blot
  - DNA Methylation in Promoter Region by Bisulfite Sequencing
  - Xist RNA-FISH
  - Telomerase Activity by TRAP Assay
  - Telomerase Assay by ELISA
  - Telomere Measurement by Real-Time qPCR
  - Telomere Restriction Fragment Measurement
  - Telomere Q-FISH
  - Flow-FISH Analysis of Telomeres
  - Library Preparation and RNA-Sequencing
  - Bioinformatics Analysis
  - Whole-Exome Sequencing
  - Sequence Alignment and Variant Calling

- QUANTIFICATION AND STATISTICAL ANALYSIS
- DATA AND CODE AVAILABILITY

SUPPLEMENTAL INFORMATION

Supplemental Information can be found online at https://doi.org/10.1016/j.celrep.2019.11.080.

ACKNOWLEDGMENTS

We thank Panpan Shi, Feixiang Ge, Kairang Jin, Renpeng Guo, Ming Zeng, and Yifei Liu for assisting with the experiments and discussion and Novogene Bioinformatics Technology Co., Ltd., for exome-seq analysis. This work was supported by the National Natural Science Foundation of China (31430052 and 31571546) and China National Key R&D Program (2018YFA0107000 and 2018YFC1003004).

AUTHOR CONTRIBUTIONS

C.T. designed the experiments, conducted the major experiments, analyzed the data, and prepared the manuscript. L.L., X.Y., H.F., X.S., L.W., H.W., and D.H. conducted part of the experiments or provided materials. L.L. conceived the project, designed the experiments, and revised the manuscript.

DECLARATION OF INTERESTS

The authors declare no competing interests.

Received: March 4, 2019
Revised: October 9, 2019
Accepted: November 19, 2019
Published: December 24, 2019

REFERENCES

Allworth, A.E., and Albertini, D.F. (1993). Meiotic maturation in cultured bovine oocytes is accompanied by remodeling of the cumulus cell cytoskeleton. Dev. Biol. *158*, 101–112.

Baerlocher, G.M., and Lansdorp, P.M. (2003). Telomere length measurements in leukocyte subsets by automated multicolor flow-FISH. Cytometry A *55*, 1–6.

Bhutani, K., Nazor, K.L., Williams, R., Tran, H., Dai, H., Džakula, Ž., Cho, E.H., Pang, A.W.C., Rao, M., Cao, H., et al. (2016). Whole-genome mutational burden analysis of three pluripotency induction methods. Nat. Commun. *7*, 10536.

Blackburn, E.H., Epel, E.S., and Lin, J. (2015). Human telomere biology: A contributory and interactive factor in aging, disease risks, and protection. Science *350*, 1193–1198.

Bru, T., Clarke, C., McGrew, M.J., Sang, H.M., Wilmut, I., and Blow, J.J. (2008). Rapid induction of pluripotency genes after exposure of human somatic cells to mouse ES cell extracts. Exp. Cell Res. *314*, 2634–2642.

Canela, A., Vera, E., Klatt, P., and Blasco, M.A. (2007). High-throughput telomere length quantification by FISH and its application to human population studies. Proc. Natl. Acad. Sci. USA *104*, 5300–5305.

Cao, S., Yu, S., Li, D., Ye, J., Yang, X., Li, C., Wang, X., Mai, Y., Qin, Y., Wu, J., et al. (2018). Chromatin Accessibility Dynamics during Chemical Induction of Pluripotency. Cell Stem Cell *22*, 529–542.

Cawthon, R.M. (2002). Telomere measurement by quantitative PCR. Nucleic Acids Res. *30*, e47.

Chen, D., Liu, W., Zimmerman, J., Pastor, W.A., Kim, R., Hosohama, L., Ho, J., Aslanyan, M., Gell, J.J., Jacobsen, S.E., and Clark, A.T. (2018). The TFAP2C-Regulated OCT4 Naive Enhancer Is Involved in Human Germline Formation. Cell Rep. *25*, 3591–3602.

Constantinescu, D., Gray, H.L., Sammak, P.J., Schatten, G.P., and Csoka, A.B. (2006). Lamin A/C expression is a marker of mouse and human embryonic stem cell differentiation. Stem Cells *24*, 177–185.

Coticchio, G., Dal Canto, M., Mignini Renzini, M., Guglielmo, M.C., Brambillasca, F., Turchi, D., Novara, P.V., and Fadini, R. (2015). Oocyte maturation: gamete-somatic cells interactions, meiotic resumption, cytoskeletal dynamics and cytoplasmic reorganization. Hum. Reprod. Update *21*, 427–454.

Edson, M.A., Nagaraja, A.K., and Matzuk, M.M. (2009). The mammalian ovary from genesis to revelation. Endocr. Rev. *30*, 624–712.

Eppig, J.J., O'Brien, M.J., Wigglesworth, K., Nicholson, A., Zhang, W., and King, B.A. (2009). Effect of *in vitro* maturation of mouse oocytes on the health and lifespan of adult offspring. Hum. Reprod. *24*, 922–928.

Findlay, J.K., Hutt, K.J., Hickey, M., and Anderson, R.A. (2015). How Is the Number of Primordial Follicles in the Ovarian Reserve Established? Biol. Reprod. *93*, 111.

Fu, H., Tian, C.L., Ye, X., Sheng, X., Wang, H., Liu, Y., and Liu, L. (2018). Dynamics of Telomere Rejuvenation during Chemical Induction to Pluripotent Stem Cells. Stem Cell Reports *11*, 70–87.

Gell, J.J., and Clark, A.T. (2018). Restoring Fertility with Human Induced Pluripotent Stem Cells: Are We There Yet? Cell Stem Cell *23*, 777–779.

Göhring, J., Fulcher, N., Jacak, J., and Riha, K. (2014). **TeloTool**: a new tool for telomere length measurement from terminal restriction fragment analysis with improved probe intensity correction. Nucleic Acids Res *42*, e21.

Gore, A., Li, Z., Fung, H.L., Young, J.E., Agarwal, S., Antosiewicz-Bourget, J., Canto, I., Giorgetti, A., Israel, M.A., Kiskinis, E., et al. (2011). Somatic coding mutations in human induced pluripotent stem cells. Nature *471*, 63–67.

Grive, K.J., and Freiman, R.N. (2015). The developmental origins of the mammalian ovarian reserve. Development *142*, 2554–2563.

Hackett, J.A., Huang, Y., Günesdogan, U., Gretarsson, K.A., Kobayashi, T., and Surani, M.A. (2018). Tracing the transitions from pluripotency to germ cell fate with CRISPR screening. Nat. Commun. *9*, 4292.

Handel, M.A., Eppig, J.J., and Schimenti, J.C. (2014). Applying "Gold Standards" to *In-Vitro*-Derived Germ Cells. Cell *159*, 216.

Hayashi, K., and Saitou, M. (2013). Generation of eggs from mouse embryonic stem cells and induced pluripotent stem cells. Nat. Protoc. *8*, 1513–1524.

Hayashi, K., Ogushi, S., Kurimoto, K., Shimamoto, S., Ohta, H., and Saitou, M. (2012). Offspring from oocytes derived from *in vitro* primordial germ cell-like cells in mice. Science *338*, 971–975.

Herrera, E., Samper, E., Martín-Caballero, J., Flores, J.M., Lee, H.W., and Blasco, M.A. (1999). Disease states associated with telomerase deficiency appear earlier in mice with short telomeres. EMBO J. *18*, 2950–2960.

Hirata, T., Amano, T., Nakatake, Y., Amano, M., Piao, Y., Hoang, H.G., and Ko, M.S. (2012). Zscan4 transiently reactivates early embryonic genes during the generation of induced pluripotent stem cells. Sci. Rep. *2*, 208.

Hochberg, Y., and Benjamini, Y. (1990). More powerful procedures for multiple significance testing. Stat. Med. *9*, 811–818.

Huang, J., Deng, K., Wu, H., Liu, Z., Chen, Z., Cao, S., Zhou, L., Ye, X., Keefe, D.L., and Liu, L. (2008). Efficient production of mice from embryonic stem cells injected into four- or eight-cell embryos by piezo micromanipulation. Stem Cells *26*, 1883–1890.

Hübner, K., Fuhrmann, G., Christenson, L.K., Kehler, J., Reinbold, R., De La Fuente, R., Wood, J., Strauss, J.F., 3rd, Boiani, M., and Schöler, H.R. (2003). Derivation of oocytes from mouse embryonic stem cells. Science *300*, 1251–1256.

Hummitzsch, K., Anderson, R.A., Wilhelm, D., Wu, J., Telfer, E.E., Russell, D.L., Robertson, S.A., and Rodgers, R.J. (2015). Stem cells, progenitor cells, and lineage decisions in the ovary. Endocr. Rev. *36*, 65–91.

Irie, N., and Surani, M.A. (2017). Efficient Induction and Isolation of Human Primordial Germ Cell-Like Cells from Competent Human Pluripotent Stem Cells. Methods Mol. Biol. *1463*, 217–226.

Irie, N., Weinberger, L., Tang, W.W., Kobayashi, T., Viukov, S., Manor, Y.S., Dietmann, S., Hanna, J.H., and Surani, M.A. (2015). SOX17 is a critical specifier of human primordial germ cell fate. Cell *160*, 253–268.

Jiang, J., Lv, W., Ye, X., Wang, L., Zhang, M., Yang, H., Okuka, M., Zhou, C., Zhang, X., Liu, L., and Li, J. (2013). Zscan4 promotes genomic stability during reprogramming and dramatically improves the quality of iPS cells as demonstrated by tetraploid complementation. Cell Res. *23*, 92–106.

Liu, L., Franco, S., Spyropoulos, B., Moens, P.B., Blasco, M.A., and Keefe, D.L. (2004). Irregular telomeres impair meiotic synapsis and recombination in mice. Proc. Natl. Acad. Sci. USA *101*, 6496–6501.

Liu, L., Bailey, S.M., Okuka, M., Muñoz, P., Li, C., Zhou, L., Wu, C., Czerwiec, E., Sandler, L., Seyfang, A., et al. (2007). Telomere lengthening early in development. Nat. Cell Biol. *9*, 1436–1441.

Liu, M., Yin, Y., Ye, X., Zeng, M., Zhao, Q., Keefe, D.L., and Liu, L. (2013). Resveratrol protects against age-associated infertility in mice. Hum. Reprod. *28*, 707–717.

Long, Y., Wang, M., Gu, H., and Xie, X. (2015). Bromodeoxyuridine promotes full-chemical induction of mouse pluripotent stem cells. Cell Res. *25*, 1171–1174.

Magnúsdóttir, E., and Surani, M.A. (2014). How to make a primordial germ cell. Development *141*, 245–252.

Magnúsdóttir, E., Dietmann, S., Murakami, K., Günesdogan, U., Tang, F., Bao, S., Diamanti, E., Lao, K., Gottgens, B., and Azim Surani, M. (2013). A tripartite transcription factor network regulates primordial germ cell specification in mice. Nat. Cell Biol. *15*, 905–915.

Mao, J., and Liu, L. (2016). Generation of iPS Cells from Granulosa Cells. Methods Mol. Biol. *1357*, 451–464.

Mao, J., Zhang, Q., Ye, X., Liu, K., and Liu, L. (2014). Efficient induction of pluripotent stem cells from granulosa cells by Oct4 and Sox2. Stem Cells Dev. *23*, 779–789.

Matoba, S., and Ogura, A. (2011). Generation of functional oocytes and spermatids from fetal primordial germ cells after ectopic transplantation in adult mice. Biol. Reprod. *84*, 631–638.

Matzuk, M.M., Burns, K.H., Viveiros, M.M., and Eppig, J.J. (2002). Intercellular communication in the mammalian ovary: oocytes carry the conversation. Science *296*, 2178–2180.

Miyauchi, H., Ohta, H., Nagaoka, S., Nakaki, F., Sasaki, K., Hayashi, K., Yabuta, Y., Nakamura, T., Yamamoto, T., and Saitou, M. (2017). Bone morphogenetic protein and retinoic acid synergistically specify female germ-cell fate in mice. EMBO J. *36*, 3100–3119.

Nagaoka, S.I., Hassold, T.J., and Hunt, P.A. (2012). Human aneuploidy: mechanisms and new insights into an age-old problem. Nat. Rev. Genet. *13*, 493–504.

Nakaki, F., Hayashi, K., Ohta, H., Kurimoto, K., Yabuta, Y., and Saitou, M. (2013). Induction of mouse germ-cell fate by transcription factors *in vitro*. Nature *501*, 222–226.

Ohinata, Y., Ohta, H., Shigeta, M., Yamanaka, K., Wakayama, T., and Saitou, M. (2009). A signaling principle for the specification of the germ cell lineage in mice. Cell *137*, 571–584.

Pasque, V., Tchieu, J., Karnik, R., Uyeda, M., Sadhu Dimashkie, A., Case, D., Papp, B., Bonora, G., Patel, S., Ho, R., et al. (2014). X chromosome reactivation dynamics reveal stages of reprogramming to pluripotency. Cell *159*, 1681–1697.

Pastor, W.A., Liu, W., Chen, D., Ho, J., Kim, R., Hunt, T.J., Lukianchikov, A., Liu, X., Polo, J.M., Jacobsen, S.E., and Clark, A.T. (2018). TFAP2C regulates transcription in human naive pluripotency by opening enhancers. Nat. Cell Biol. *20*, 553–564.

Picelli, S., Faridani, O.R., Björklund, A.K., Winberg, G., Sagasser, S., and Sandberg, R. (2014). Full-length RNA-seq from single cells using Smart-seq2. Nat. Protoc. *9*, 171–181.

Polejaeva, I.A., Chen, S.H., Vaught, T.D., Page, R.L., Mullins, J., Ball, S., Dai, Y., Boone, J., Walker, S., Ayares, D.L., et al. (2000). Cloned pigs produced by nuclear transfer from adult somatic cells. Nature *407*, 86–90.

Poon, S.S., Martens, U.M., Ward, R.K., and Lansdorp, P.M. (1999). Telomere length measurements using digital fluorescence microscopy. Cytometry *36*, 267–278.

Qing, T., Liu, H., Wei, W., Ye, X., Shen, W., Zhang, D., Song, Z., Yang, W., Ding, M., and Deng, H. (2008). Mature oocytes derived from purified mouse fetal germ cells. Hum. Reprod. *23*, 54–61.

Sasaki, K., Yokobayashi, S., Nakamura, T., Okamoto, I., Yabuta, Y., Kurimoto, K., Ohta, H., Moritoki, Y., Iwatani, C., Tsuchiya, H., et al. (2015). Robust *In Vitro* Induction of Human Germ Cell Fate from Pluripotent Stem Cells. Cell Stem Cell *17*, 178–194.

Shen, W., Zhang, D., Qing, T., Cheng, J., Bai, Z., Shi, Y., Ding, M., and Deng, H. (2006). Live offspring produced by mouse oocytes derived from premeiotic fetal germ cells. Biol. Reprod. *75*, 615–623.

Suzuki, A., Hirasaki, M., Hishida, T., Wu, J., Okamura, D., Ueda, A., Nishimoto, M., Nakachi, Y., Mizuno, Y., Okazaki, Y., et al. (2016). Loss of MAX results in meiotic entry in mouse embryonic and germline stem cells. Nat. Commun. *7*, 11056.

Wakayama, T., Perry, A.C., Zuccotti, M., Johnson, K.R., and Yanagimachi, R. (1998). Full-term development of mice from enucleated oocytes injected with cumulus cell nuclei. Nature *394*, 369–374.

Yamaguchi, S., Hong, K., Liu, R., Shen, L., Inoue, A., Diep, D., Zhang, K., and Zhang, Y. (2012). Tet1 controls meiosis by regulating meiotic gene expression. Nature *492*, 443–447.

Yamashiro, C., Sasaki, K., Yabuta, Y., Kojima, Y., Nakamura, T., Okamoto, I., Yokobayashi, S., Murase, Y., Ishikura, Y., Shirane, K., et al. (2018). Generation of human oogonia from induced pluripotent stem cells *in vitro*. Science *362*, 356–360.

Ye, J., Ge, J., Zhang, X., Cheng, L., Zhang, Z., He, S., Wang, Y., Lin, H., Yang, W., Liu, J., et al. (2016). Pluripotent stem cells induced from mouse neural stem cells and small intestinal epithelial cells by small molecule compounds. Cell Res. *26*, 34–45.

Zeng, M., Sheng, X., Keefe, D.L., and Liu, L. (2017). Reconstitution of ovarian function following transplantation of primordial germ cells. Sci. Rep. *7*, 1427.

Zhang, H., and Liu, K. (2015). Cellular and molecular regulation of the activation of mammalian primordial follicles: somatic cells initiate follicle activation in adulthood. Hum. Reprod. Update *21*, 779–786.

Zhao, Y., Zhao, T., Guan, J., Zhang, X., Fu, Y., Ye, J., Zhu, J., Meng, G., Ge, J., Yang, S., et al. (2015). A XEN-like State Bridges Somatic Cells to Pluripotency during Chemical Reprogramming. Cell *163*, 1678–1691.

Zhao, T., Fu, Y., Zhu, J., Liu, Y., Zhang, Q., Yi, Z., Chen, S., Jiao, Z., Xu, X., Xu, J., et al. (2018). Single-Cell RNA-Seq Reveals Dynamic Early Embryonic-like Programs during Chemical Reprogramming. Cell Stem Cell *23*, 31–45.

Zhou, Q., Wang, M., Yuan, Y., Wang, X., Fu, R., Wan, H., Xie, M., Liu, M., Guo, X., Zheng, Y., et al. (2016). Complete Meiosis from Embryonic Stem Cell-Derived Germ Cells *In Vitro*. Cell Stem Cell *18*, 330–340.

Zong, C., Lu, S., Chapman, A.R., and Xie, X.S. (2012). Genome-wide detection of single-nucleotide and copy-number variations of a single human cell. Science *338*, 1622–1626.

Zuo, B., Yang, J., Wang, F., Wang, L., Yin, Y., Dan, J., Liu, N., and Liu, L. (2012). Influences of lamin A levels on induction of pluripotent stem cells. Biol. Open *1*, 1118–1127.

STAR★METHODS

KEY RESOURCES TABLE

REAGENT or RESOURCE	SOURCE	IDENTIFIER
Antibodies		
Zscan4	Millipore	Cat#: AB4340
Pan-Kcr	PTM biolabs	Cat#: PTM-502
Oct4	Santa Cruz	Cat#: sc5279
β-Actin	Abmart	Cat#: P30002
Ki67	Millipore	Cat#: AB9260
LaminA	Abcam	Cat#: ab26300
Foxl2	Abcam	Cat#: ab5096
H3K27me3	Millipore	Cat#: 07-499
Sox2	Millipore	Cat#: AB5603
Nanog	Abcam	Cat#: ab80892
Lin28	CST	Cat#: 3978S
βIII-tubulin	Chemicon	Cat#: CBL412
α-SMA	Abcam	Cat#: ab5694
AFP	Dako	Cat#: DAK-N1501
Nestin	Millipore	Cat#: MAB353
α-Tubulin	Sigma	Cat#: SAB4800087
SCP1	Abcam	Cat#: ab15090
SCP3	Novus	Cat#: NB300-230
MLH1	BD	Cat#: 550838
Texas Red-conjugated Phalloidin	Abcam	Cat#: ab176757
anti-SSEA1 conjugated with magnetic beads	Miltenyi	Cat#: 130-094-530
anti-SSEA1 conjugated with Alexa Fluor 647	eBioscience	Cat#: 50-8813-42
anti-CD61 conjugated with PE	BioLegend	Cat#: 104307
FITC Goat Anti-Mouse IgG (H+L)	Jackson	Cat#: 115-095-003
Alexa Fluor® 594 Goat Anti-Rabbit IgG (H+L)	Jackson	Cat#: 111-585-003
Alexa Fluor® 488 Goat Anti-Rabbit IgG (H+L)	Life	Cat#: A11008
Alexa Fluor® 594 Goat Anti-Mouse IgG (H+L)	Life	Cat#: A-11005
Alexa Fluor® 594 Donkey Anti-Goat IgG (H+L)	Abcam	Cat#: ab150132
Goat anti-Rabbit IgG-HRP	GE Healthcare	Cat#: NA934V
Goat anti-Mouse IgG (H+L)/HRP	ZSGB-BIO	Cat#: ZB2305
Bacterial and Virus Strains		
Trans1-T1 Phage Resistant Chemically Competent Cell	Transgene	Cat#: CD501-03
Chemicals, Peptides, and Recombinant Proteins		
Y27632	Selleck	Cat#: S1049
PD0325901	Miltenyi	Cat#: 04-0006
CHIR99021	Selleck	Cat#: S1263
ESGRO (LIF)	Millipore	Cat#: ESG1107
Human bFGF	PeproTech	Cat#: 96-100-18B
VPA	Sigma	Cat#: P4543
Repsox	Selleck	Cat#: S7223
Parnate	Sigma	Cat#: P8511
Forskolin	Selleck	Cat#: S2449
AM580	Tocris	Cat#: 0760-10

(*Continued on next page*)

Continued

REAGENT or RESOURCE	SOURCE	IDENTIFIER
EPZ004777	Selleck	Cat#: S7353
DZNep	Selleck	Cat#: S7120
5-aza-dC	Sigma	Cat#: A3656
SGC0946	Selleck	Cat#: S7079
Crotonic acid	Millipore	Cat#: 802650
Human plasma fibronectin (FN)	Millipore	Cat#: FC010
Human Activin A	PeproTech	Cat#: 120-14
Human BMP4	PeproTech	Cat#: 120-05
Murine SCF	PeproTech	Cat#: 250-03
Murine EGF	PeproTech	Cat#: 315-09
Vitamin C (Vc)	Sigma	Cat#: A8960
Critical Commercial Assays		
Serum follicle-stimulating hormone ELISA Kit	EastBiopharm	Cat#: CK-E20381
Estradiol (E2) ELISA Kit	EastBiopharm	Cat#: CK-E20419
Anti-Müllerian hormone (AMH) ELISA Kit	EastBiopharm	Cat#: CK-E90200
RNeasy Plus Mini Kit	QIAGEN	Cat#: 74134
DNeasy Blood & Tissue Kit	QIAGEN	Cat#: 69504
EpiTect Bisulfite Kit	QIAGEN	Cat#: 59104
QIAquick Gel Extraction Kit	QIAGEN	Cat#: 28704
pEASY-T1 Simple Cloning Kit	Transgene	Cat#: CT111
TeloChaser Telomerase assay kit	MD Biotechnology	Cat#: T0001
Mouse Telomerase (TE) ELISA kit	CUSABIO	Cat#: CSB-E08022
TeloTAGGG Telomere Length Assay	Roche	Cat#: 12209136001
TruSeq PE Cluster Kit	Illumina	Cat#: PE-201-5001
TruePrep DNA Library Prep Kit V2 for Illumina®	Vazyme Biotech	Cat#: TD503-02
Deposited Data		
RNA-seq Data	This paper	GSE127833
Whole exome-seq Data	This paper	PRJNA559066
Experimental Models: Cell Lines		
gPSC lines	This paper	NA
Female ESCs	This paper	NA
OG4 ESCs	Fu et al., 2018	NA
Experimental Models: Organisms/Strains		
Oct4-GFP (OG2) mice	Jackson	#004654
Nu/Nu mice	Vital River	#403
NOD-SCID mice	Vital River	#406
Albino Bal-b/c mice	Vital River	#401
Albino ICR mice	Vital River	#201
Albino Kunming (KM) mice	Vital River	#202
Probe		
Xist RNA-FISH probe	Biosearch Technologies	Cat#: SMF-3011-1
FITC-labeled $(CCCTAA)_3$ peptide nucleic acid (PNA) probe	Panagene	Cat#: F1001
Cy3-labeled $(CCCTAA)_3$ peptide nucleic acid (PNA) probe	Panagene	Cat#: F1002
Software and Algorithms		
FlowJo	Tree Star Inc	Version 10.2
GraphPad Prism software	GraphPad Software	Version 7
TeloTool software	Gohring et al., 2014	Version 1.3.0.0

(*Continued on next page*)

Continued

REAGENT or RESOURCE	SOURCE	IDENTIFIER
TFL-TELO program	Kindly provided by Peter Lansdorp, Terry Fox Laboratory	N/A
RStudio	RStudio	R version 3.4.2
R package of "pheatmap," "cor" and "ggplot2"	Bioconductor	3.6.0
StatView software	SAS Institute Inc.	N/A

LEAD CONTACT AND MATERIALS AVAILABILITY

Further information and requests for resources and reagents should be directed to and will be fulfilled by the Lead Contact, Lin Liu (liulin@nankai.edu.cn). This study did not generate new unique reagents. All unique/stable reagents generated in this study are available from the Lead Contact with a completed Materials Transfer Agreement.

EXPERIMENTAL MODEL AND SUBJECT DETAILS

Mice

Use of mice for this research was approved by the Nankai University Animal Care and Use Committee. All mice used in this study were taken care of and operated according to the relevant regulations. Mice at the age of 4-8 weeks old were healthy, housed and cared in individually ventilated cages (IVCs) on a standard 12 h light: 12 h dark cycle in the sterile Animal Facility at College of Life Sciences. Male and female Oct4-GFP (OG2) mice (C57BL6 X CBA, JAX stock #004654) that carry Oct4 distal promoter-driven GFP were purchased from Model Animal Research Center of Nanjing University. Nu/Nu mice (Female, #403), NOD-SCID mice (Female, #406), albino BALB/c mice (Female, #401), albino ICR mice (Male and female, #201) and albino Kunming (KM) mice (Female, #202) were purchased from Beijing Vital River Laboratory Animal Technology Co., Ltd.

Isolated and Primary Cultured Mouse Embryonic Fibroblasts

MEFs were derived from E13.5 embryos isolated from ICR mice by caesarean section and washed in phosphate-buffered saline (PBS). Heads and visceral tissues were removed, and remaining tissue washed in PBS, then submerged in 0.25% trypsin-EDTA (0.25% TE, Invitrogen) and incubated at 37°C for 10 min. Tissue was pipetted repeatedly to aid dissociation, washed then dissociated cells added to MEF medium and plated (passage 0, P0). MEFs were genotyped by *Sry* gene to determine the Sex (Forward primer: CATCGGAGGGCTAAAGTGTC; Reserve primer: TCCAGTCTTGCCTGTATGTG). MEF medium contains DMEM (Invitrogen) supplemented with 10% Fetal Bovine Serum (FBS, Hyclone), 1 mM L-glutamine (Invitrogen), 1% nonessential amino acid stock (NEAA, Sigma), and 50 units/ml penicillin and 50 μg/ml streptomycin (2A, Invitrogen). Cells were cultured at 37°C in 5% CO_2 incubator with humidified air (Thermo Scientific USA).

Mouse ESC Lines

ESC lines were established and characterized based on the method described (Huang et al., 2008). Blastocysts were isolated from the uterine horns of pregnant females at Embryo (E) day 3.5 using a dissection microscope in HKSOM and plated onto mitomycin C-treated MEF cells served as feeders in KSR/DMEM added with PD0325901 and LIF (K/DL) medium and cultured for 7 days to form outgrowths. Emerging ICM outgrowths were directly picked into serum/LIF (S/L) medium on feeders to establish stable ESC lines. Established ESC lines were genotyped by *Sry* gene to determine the sex. Female ESC lines were maintained by dissociating cells with 0.25% TE (Invitrogen) every 2∼3 days and re-plated onto feeder cells. K/DL medium contains knockout DMEM (Invitrogen) supplemented with 20% Knockout serum replacement (KSR, Invitrogen), 1 mM L-glutamine, 1% nonessential amino acid stock, 50 units/ml penicillin and 50 μg/ml streptomycin (2A, Invitrogen), 0.1 mM β-mercaptoethanol (Invitrogen), 1 μM PD0325901 (Miltenyi) and 1000 IU/ml mouse LIF (mLIF, Millipore). S/L medium (ESC culture medium) contains knockout DMEM supplemented with 15% FBS (ES quality, Hyclone), 1 mM L-glutamine, 1% nonessential amino acid stock, 50 units/ml penicillin and 50 μg/ml streptomycin, 0.1 mM β-mercaptoethanol, and 1000 IU/ml mLIF. ESCs were cultured at 37°C in 5% CO_2 incubator with humidified air.

Isolated and Primary Cultured Granulosa Cells

The method of isolation of GCs was described previously (Mao and Liu, 2016). Briefly, pregnant mare serum gonadotropin (PMSG, Millipore, 5 IU per mouse) was injected into the abdominal cavity of 6-week-old female OG2 mice 46 h prior to isolating GCs. The mice were humanely sacrificed and the ovaries dissected. To isolate GCs, an insulin syringe was used to puncture visible follicles on the surface of ovaries under a stereomicroscope to release GCs into culture medium. The maturing or mature follicles in principle do not contain the primordial oocytes. In addition, 40 μm Cell Strainer were used to wipe off oocytes if any. Then, the freshly isolated GCs were washed in PBS and cultured in S/L medium, and the medium was changed every 48 h. Cells were cultured at 37°C in 5% CO_2 incubator with humidified air.

METHOD DETAILS

Proliferation Curve of Granulosa Cells

The primary cultured GCs for 7 days (P0) were dissociated with 0.25% TE, washed, centrifuged, and resuspended in S/L medium, followed by seeding at a density of 10^5 cells per well in 6 well plate in S/L medium added with 10 μM Y27632 (Rock inhibitor, Rocki, Selleck) for only 24 h to facilitate cell adherence. Next day, the culture (considered as P1) was changed into S/L medium without Y27632. At various days, the cultured GCs were dissociated into single cells by 0.25% TE, washed, centrifuged, resuspended in PBS, and counted by Hemocytometer.

Induction of gPSCs from Granulosa Cells

GCs were freshly isolated from OG2 mice that carry Oct4 distal promoter-driven GFP. Induction to pluripotent stem cells (PSCs) by small chemicals was performed based on the method described (Zhao et al., 2015), with modifications (Fu et al., 2018). The primary cultured GCs for 7 days (P0) were dissociated with 0.25% TE, washed, centrifuged, and resuspended in S/L medium, followed by seeding at a density of 10^5 cells per well in 6 well plate in S/L medium added with 10 μM Y27632 for only 24 h or without Y27632 served as control. Next day (0 D of induction), the culture (considered as P1) was changed into the Stage 1 induction medium for CiPSC induction.

On 0-12 D (The first part of Stage 1), the induction medium contained 100 ng/ml bFGF (PeproTech), 0.5 mM VPA (Sigma), 20 μM CHIR99021 (Selleck), 10 μM Repsox (Selleck), 5 μM Parnate (Sigma), 50 μM Forskolin (Selleck), 0.05 μM AM580 (Tocris) and 5 μM EPZ004777 (Selleck). During 12-16 D (The second part of Stage 1), concentrations of bFGF, CHIR99021, and Forskolin were reduced to 25 ng/ml, 10 μM, and 10 μM, respectively. On 16-28 D (Stage 2), the induction medium contains 25 ng/ml bFGF, 0.5 mM VPA, 10 μM CHIR99021, 10 μM Repsox, 5 μM Parnate, 10 μM Forskolin, 0.05 μM AM580, 0.05 μM DZNep (Selleck), 0.5 μM 5-aza-dC (Sigma), and 5 μM SGC0946 (Selleck). On 28 D (Stage 3), the culture was transferred into 2i/L medium. 2i/L medium contains a 1:1 mixture of DMEM/F12 (Invitrogen) supplemented with N2 and B27 (Invitrogen), 1 mM L-glutamine, 1% nonessential amino acid stock, 50 units/ml penicillin and 50 μg/ml streptomycin, 0.1 mM β-mercaptoethanol, 1000 IU/ml mLIF, 1 μM PD0325901 and 3 μM CHIR99021. After 8-12 days, Oct4 GFP-positive, GCs-derived PSCs (gPSC) primary colonies emerged and were then picked up for expansion by culture in S/L + 2i medium on feeders.

In comparison experiments by treatment with or without crotonic sodium (CS, crotonic acid (Millipore), added with 1 N NaOH to adjust the pH = 7.0) during induction, 7 mM CS was added into induction medium during Stage 2 from 16 D to 28 D. Oct4 GFP-positive cells emerged about from 32 D-36 D, and clones can be picked up at 40 D. For FACS analysis of reprogramming efficiency, cells at 40 D of induction were collected and washed three times with PBS and FACS analysis performed using a Flow Cytometer (Aria III, BD Biosciences).

Induction of PGC-like Cells

Induction of PGC-like cells (PGCLCs) from ESCs/gPSCs was based on the method described previously (Hayashi and Saitou, 2013). ESCs and gPSCs at passage 7-8 were transferred into feeder-free N2B27+t2iL medium (in 2iL medium, the concentration of PD0325901 was reduced from 1 μM to 0.4 μM) and maintained for 3-5 passages. EpiLCs were induced by plating 1.0×10^5 female ESCs/gPSCs on the wells of a 12-well plate coated with human plasma fibronectin (FN, 16.7 μg/ml, Millipore) in N2B27 medium containing activin A (20 ng/ml, PeproTech), bFGF (12 ng/ml), and 1% KSR for 2 days. The medium was changed every day. The PGCLCs were induced for 4 days under floating conditions by plating 3.0×10^3 EpiLCs in the wells of a low-cell-binding U-bottom 96-well Lipidure-Coat plate (Corning) in GK15 medium (GK15 medium contains GMEM (Invitrogen) added with 15% KSR, 1 mM sodium pyruvate, 1 mM L-glutamine, 1% nonessential amino acid stock, 50 units/ml penicillin and 50 μg/ml streptomycin, and 0.1 mM β-mercaptoethanol) in the presence of the cytokines BMP4 (500 ng/ml, PeproTech), 1000 IU/ml mLIF, SCF (100 ng/ml, PeproTech) and EGF (50 ng/ml, PeproTech). Integrin-β3- (CD61) and SSEA1-double positive ESCs/gPSCs-derived PGCLCs were sorted by flow cytometer. Dissociated cells were incubated with anti-integrin-β3 (CD61) antibody and anti-SSEA1 antibody conjugated with PE (Phycoerythrin, Red color) and Alexa Fluor 647, respectively. After being washed in PBS supplemented with 0.1% bovine serum albumin (BSA, Sigma), the cells were sorted and analyzed using a flow cytometer (Aria III; BD Biosciences).

Induction of Meiosis and Folliculogenesis

Induction of meiosis and folliculogenesis was achieved by aggregation of PGCLCs or PGCs served as a control with E12.5 gonadal somatic cells followed by transplantation of the aggregates into kidney capsules to generate reconstituted ovaries (rOvaries). To obtain E12.5 gonad somatic cells *in vivo*, female E12.5 gonads were collected from E12.5 embryos obtained by intercrosses of albino ICR mice. The mesonephros were surgically separated from the gonads using insulin syringe. Gonads were dissociated with 0.05% TE by incubation at 37°C for 10 min, washed with MEF medium, and collected by centrifugation. Large clumps of cells were removed using a cell strainer (BD Biosciences). Endogenous PGCs in the dissociated gonadal cells were removed or collected by magnetic cell sorting using anti-SSEA1 antibody conjugated with magnetic beads (Miltenyi, see below). The sorted gonadal somatic cells and FACS-sorted PGCLCs or PGCs from OG2 mice were plated in the wells of a low-cell-binding U-bottom 96-well Lipidure-Coat plate in MF10 medium (MF10 medium contains M199 (Sigma) added with 10% FBS, 1 mM L-glutamine, 1% nonessential amino acid stock, and 50 units/ml penicillin and 50 μg/ml streptomycin) with or without 50 μg/ml Vitamin C (Vc, Sigma) or/and 10 μM Rocki (Zeng et al.,

2017). Each aggregate contained 20,000 E12.5 PGCs or PGCLCs and 100,000 gonadal somatic cells. For negative control (pseudo-rOvary), 100,000 E12.5 gonadal somatic cells only without PGCs were aggregated in MF10 medium supplemented with 50 μg/ml Vitamin C and 10 μM Rocki.

Magnetic Activated Cell Sorting

Magnetic activated cell sorting (MACS) was performed according to the manufacturer's instructions (Miltenyi). Briefly, dissociated gonadal cells were incubated with anti-SSEA1 antibody conjugated with magnetic beads. Cell suspensions were washed in PBS supplemented with 0.5% BSA and 2 mM EDTA and applied to an MS column (Miltenyi) to remove SSEA1-positive PGCs. Gonadal somatic cells were collected in the flow-through portions. To verify that SSEA1 negative cells do not contain PGCs, SSEA1/ CD61 double staining was used as markers to detect PGCs by FACS. More than 99.99% cells did not express SSEA1 and CD61, indicating the purity of embryonic gonadal somatic cells.

Kidney Capsule Transplantation

Kidney capsule transplantation was performed based on the methods described (Qing et al., 2008; Zeng et al., 2017). Briefly, one or two aggregates were implanted in the "pocket" which was made between the kidney capsule and kidney tissue of a bilaterally ovariectomized recipient mouse. Transplantation procedure was completed in 5 min for each mouse. Meiosis and folliculogenesis were achieved in the rOvaries 28 days following transplantation of the aggregates.

In Vitro Maturation and *In Vitro* Fertilization

The rOvaries were dissected from the recipient mouse kidney capsule, and fully-grown GV oocytes were collected under a microscope by pricking follicles using insulin syringe in *in vitro* maturation (IVM) medium. Oocytes were matured *in vitro* by culture in IVM medium for 17-18 h at 37°C (Eppig et al., 2009). IVM medium contains α-MEM (Invitrogen) added with 5% FBS, 0.24 mM sodium pyruvate, 1 IU/ml PMSG and 1.5 IU/ml human chorionic gonadotropin (hCG, Sigma). Oocytes at MII, determined by extrusion of the first polar body, were subjected to IVF. With this IVM method, 80% of maturation rate was routinely obtained for oocytes collected *in vivo*.

For *in vitro* fertilization (IVF), spermatozoa were collected from the cauda epididymis of ICR males, capacitated by incubation for 2 h in HTF (Origio), and then incubated with the matured oocytes for 6 h. The zygotes were transferred into human G-1 plus medium (Vitrolife). Embryos that reached the 2-cell stage after 24 h culture were transferred into the oviducts of E0.5 pseudo pregnant mice or cultured in $KSOM_{AA}$ medium for blastocyst transfer into the uterus of E2.5 pseudo-pregnant mice, and newborns were normally delivered on E19.5. Pups were identified initially by coat color. The contribution of E12.5 PGCs, ESCs or gPSCs to various tissues of pups was confirmed by GFP primer and by standard DNA microsatellite genotyping analysis using D8Mit94 and D12Mit136 primers (Table S2).

Embryoid Body Formation Assay

ESCs and gPSCs were removed off feeder cells twice based on their differences in the adherence to the bottom of dish. The ESCs or gPSCs were diluted to 4×10^4/ml. Every 30 μL was pipetted to form a hanging drop on the cover of the 100 mm dish. Embryoid body (EBs) formed on day 4 and were transferred into 6-well plates for adherent culture, and fixed for immunofluorescence staining using markers of three embryonic germ layers on day 15.

Teratoma Formation Assay

1×10^6 ESCs and gPSCs were injected subcutaneously into about 6-week-old female Nu/Nu mice. About 4 weeks after injection, the mice were humanely sacrificed, and the teratomas were excised, fixed in 4% paraformaldehyde, dehydrated in gradient ethanol, embedded in paraffin, and sectioned for histological examination by hematoxylin and eosin (H&E) staining.

Production of Chimeras and Genotyping

Approximately 10-15 ESCs or gPSCs at P8-12 were injected into 4-8-cell embryos of BALB/c mice as hosts using a Piezo injector as described (Huang et al., 2008). Injected embryos were cultured overnight in $KSOM_{AA}$ medium. Blastocysts were transferred into uterine horns of E2.5 surrogate mice. Pregnant females delivered pups naturally at about E19.5. Pups were identified initially by coat color. The contribution of ESCs or gPSCs to various tissues in chimeras was confirmed by standard DNA microsatellite genotyping analysis using D12Mit136 primers (Table S2). Chimeras were mated with albino strain ICR mice to further examine their germline transmission competence.

Follicle Count

The aggregate-formed rOvaries were carefully retrieved and subsequently dehydrated with graded alcohols, cleared in xylene, and embedded in paraffin wax. The serial sections (5 μm) from each rOvary were aligned in order on glass microscope slides, stained with H&E and analyzed for the number of follicles at different developmental stages in every fifth section with random start in the first five sections. The total number of follicles per rOvary was calculated by combining the counts of every fifth section throughout the whole rOvary (Liu et al., 2013). The follicles were categorized into primordial or primary, secondary, and antral or mature and

atretic accordingly. Primordial, primary, and intermediate-stage follicles were identified by the presence of an oocyte surrounded by a single layer of flat, squamous, or cuboidal cells. Secondary follicles were characterized as having more than one layer of GCs with no visible antrum. Antral or mature follicles possessed small areas of follicular fluid (antrum) or a single large antral space. Only those follicles containing an oocyte with a clearly visible nucleus were scored.

Immunofluorescence Microscopy

Cells were washed twice in PBS, fixed in freshly prepared 3.7% paraformaldehyde for 30 min on ice, washed once in PBS and permeabilized in 0.1% Triton X-100 in blocking solution (3% goat serum plus 0.1% BSA in PBS) for 30 min at room temperature, then washed three times in PBS, and left in blocking solution for 2 h. Cells were incubated overnight at 4°C with primary antibodies anti-Oct4, Nanog, Gata4, LaminA, Foxl2, Ki67, H3K27me3, βIII-tubulin, AFP, α-SMA, Nestin, Zscan4, or Pan-Kcr in blocking solution. Cells were washed three times (each for 15 min) with blocking solution, and incubated for 2 h with secondary antibodies at room temperature. FITC-goat anti-mouse IgG (H+L), Alexa Fluor® 594 goat anti-rabbit IgG (H+L), or Alexa Fluor® 594 donkey anti-goat IgG (H+L) diluted 1:200 with blocking solution were used. Samples were washed, and counterstained with 0.5 μg/ml DAPI (Roche) in Vectashield (Vector) mounting medium. Fluorescence was detected and imaged using Axio-Imager Z2 Fluorescence Microscope (Carl Zeiss).

Fluorescence Microscopy of Teratoma or Tissue Sections

Briefly, after being deparaffinized, rehydration, and wash in 0.01 M PBS (pH = 7.2), sections were subjected to high pressure antigen recovery sequentially in 0.01 M citrate buffer (pH = 6.0) for 3 min, incubated with blocking solution (5% goat serum and 0.1% BSA in PBS) for 2 h at room temperature, and then with the diluted primary antibodies overnight at 4°C. The following primary antibodies were used for immunocytochemistry: anti-Nestin, α-SMA and AFP. Blocking solution without the primary antibody served as negative control. After washing with PBS, sections were incubated with appropriate secondary antibodies, FITC-goat anti-mouse IgG (H+L) or AlexaFluor® 594 goat anti-rabbit IgG (H+L). Nuclei were stained with 0.5 μg/ml DAPI in Vectashield mounting medium. Fluorescence was detected and imaged using Axio-Imager Z2 Fluorescence Microscope (Carl Zeiss).

Fluorescence Microscopy of Meiocyte Spreads

Surface spreading of meiocytes was prepared by a drying-down technique and stained for synaptonemal complexes (Liu et al., 2004). PGC-aggregates, PGCLC-aggregates and E17.5 ovaries were collected, minced with two forceps and dissociated by pipetting in 0.05% TE. After incubation for 7 min at 37°C, cell suspensions were mixed with an equal volume of FBS, centrifuged for 5 min and resuspended in 100 mM sucrose. The cell suspension was spread onto glass slide by dipping onto a thin layer of fixative (1% paraformaldehyde, 0.15% Triton X-100 and 3 mM dithiothreitol, pH = 9.2). The glass slides were maintained overnight in a humidified box at 4°C. The slides were washed in water containing 0.4% Photo-flow (Kodak), and completely dried at room temperature. Dried slides were washed with 0.1% Triton X-100/PBS (PBST) for 10min, and incubated with antibody dilution buffer (ADB, 3% BSA, 2% goat serum/PBST) for 1 h at room temperature. Spreads were then incubated with anti-SCP1, SCP3 or MLH1 antibody in ADB at 4°C overnight, washed three times, then incubated with appropriate secondary antibodies, AlexaFluor® 488 Goat anti-Rabbit IgG (H+L), AlexaFluor® 594 Goat anti-Rabbit IgG (H+L), FITC Goat anti-Mouse IgG (H+L) or AlexaFluor® 594 Goat anti-Mouse IgG (H+L), washed, added with DAPI, and mounted in Vectashield mounting medium (Vector Laboratories). Immunofluorescence was detected using Axio-Imager Z2 Fluorescence Microscope. MLH1 foci were counted as described (Liu et al., 2004).

Immunofluorescence Microscopy of Spindle

Tubulin, actin filament and chromatin were stained and observed by immunofluorescence microscopy, as described previously (Allworth and Albertini, 1993). Denuded MII oocytes were fixed and extracted for 30 min at 37°C in a microtubule-stabilizing buffer. Oocytes were washed extensively and blocked overnight at 4°C in wash medium (PBS, supplemented with 0.02% NaN_3, 0.01% Triton X-100, 0.2% non-fat dry milk, 2% goat serum, 2% BSA and 0.1 M glycine). Afterward, oocytes were incubated with anti-α-Tubulin-FITC antibody at 37°C for 2 h. After washing, samples were stained for actin filaments with Texas Red-conjugated Phalloidin (1:1000) for 30 min, washed again and counterstained with 0.5 μg/ml DAPI (Roche) in Vectashield (Vector) mounting medium. Fluorescence was detected and imaged using Axio-Imager Z2 Fluorescence Microscope (Carl Zeiss).

Hormone Assays

Serum follicle-stimulating hormone (FSH), estradiol (E2) and anti- Müllerian hormone (AMH) levels were assayed by ELISA kit (CK-E20381, CK-E20419 and CK-E90200, Hangzhou EastBiopharm CO., LTD). Quality control serum, sterilized distilled water, and five series diluted standard samples for a standard curve were tested for each serum sample. The intra- and inter-assay coefficients of variability for AMH, FSH, and E2 were below 8% and 12%.

Gene Expression Analysis by Real-Time qPCR

Total RNA was purified using RNA mini kit (QIAGEN), treated with DNase I (QIAGEN), and the cDNA was generated from 2 μg RNA using Oligo (dT)18 primer (Takara) and M-MLV Reverse Transcriptase (Invitrogen). Real-time quantitative PCR (qPCR) reactions were set up in duplicate with the FS Universal SYBR Green Master (Roche) and carried out on an iCycler MyiQ2 Detection System

(Bio-Rad). All reactions were carried out by amplifying target genes and internal control in the same plate. Each sample was repeated three times and normalized using *Gapdh* as the internal control. The amplification was performed for primary denaturation at 95°C for 10 min, then 40 cycles of denaturation at 95°C for 15 s, annealing and elongation at 58°C for 1 min, and the last cycle under 55-95°C for dissociation curve. Relative quantitative evaluation of target gene was determined by comparing the threshold cycles. Primers (Table S3) were confirmed for their specificity with dissociation curves.

Western Blot

Cells were washed twice in PBS, collected, and lysed in cell lysis buffer on ice for 30 min and then sonicated for 1 min at 60 of amplitude at 2 s intervals. After centrifugation at 10,000 *g* at 4°C for 10 min, supernatant was transferred into new tubes. The concentration of the protein sample was measured by bicinchoninic acid, and protein samples boiled in SDS sample buffer at 95°C for 10 min. Protein (10 μg) of each cell extract was resolved by 10% Acr-Bis SDS-PAGE and transferred to polyvinylidene difluoride membranes (PVDF, Millipore). Nonspecific binding was blocked by incubation in 5% skim milk or 5% BSA in TBST at room temperature for 2 h. Blots were then probed with primary antibodies overnight by incubation at 4°C with Oct4, Nanog, Sox2, Lin28, Zscan4, Pan-Kcr, LaminA, PCNA, Bcl-2, Bcl-xL, Bad, Bax or β-Actin served as loading control. Immunoreactivity bands were then probed for 2 h at room temperature with the appropriate horseradish peroxidase (HRP)-conjugated secondary antibodies, HRP-goat anti-rabbit IgG, or HPR-goat anti-mouse IgG (H+L). Protein bands were detected by Chemiluminescent HRP substrate (WBKLS0500, Millipore).

DNA Methylation in Promoter Region by Bisulfite Sequencing

Genomic DNA was extracted from samples of GCs, ESCs and gPSCs using DNeasy Tissue Kit (QIAGEN) according to the manufacturer's instructions. Bisulfite treatment of DNA was performed with the EpiTect Bisulfite Kit (QIAGEN). Bisulfite converted DNA was amplified by PCR, using HS Taq DNA Polymerase (QIAGEN). Thermal cycling was carried out with a 10 min denaturation step at 94°C, followed by 35 three-step cycles (30 s at 94°C, 30 s at 55-58°C and 30 s at 72°C) and final incubation at 72°C for 10 min. PCR products were recovered from stained gels (QIAquick Gel Extraction Kit, QIAGEN), cloned into a pGEM-T Easy vector (Promega) and then sequenced using T7 or SP6 primers using an ABI 3730 capillary genetic analyzer (Applied Biosystems) by BigDye terminator sequencing chemistry. Bisulfite efficiency as the fraction of modified cytosines in non-CpG sequences exceeded 98%.

Xist RNA-FISH

Xist RNA-FISH was performed according to the manufacturer's instructions (Biosearch Technologies). Growing cells were washed with PBS and fixed with 10% formaldehyde for 10 min at room temperature. After being washed twice with PBS, cells were immersed in 70% ethanol for at least one hour at 4°C. Wash Buffer A (SMF-WA1-60, Biosearch Technologies) were added to cells and incubated at room temperature for 5 min. After incubation with the Hybridization Buffer (SMF-HB1-10, Biosearch Technologies) containing *Xist* RNA-FISH probe (SMF-3011-1, Biosearch Technologies) for 12-16 h at 37°C, cells were washed with Wash Buffer A and Wash Buffer B (SMF-WA1-20, Biosearch Technologies). Nuclei were stained with 0.5 μg/ml DAPI in Vectashield mounting medium. Fluorescence was detected and imaged using Axio-Imager Z2 Fluorescence Microscope.

Telomerase Activity by TRAP Assay

Telomerase activity was determined by the Stretch PCR method according to manufacturer's instruction using TeloChaser Telomerase assay kit (T0001, MD Biotechnology). About 2.5 × 10^4 cells from each sample were lysed. Lysis buffer served as negative controls. PCR products of cell lysate were separated on non-denaturing TBE-based 12% polyacrylamide gel electrophoresis and visualized by ethidium bromide (EB) staining.

Telomerase Assay by ELISA

Telomerase level was determined by ELISA method according to manufacturer's instruction using Mouse Telomerase (TE) ELISA kit (CSB-E08022m, CUSABIO).

Telomere Measurement by Real-Time qPCR

Genome DNA was prepared using DNeasy Blood & Tissue Kit (QIAGEN, Valencia, CA). Average telomere length was measured from total genomic DNA using a real-time PCR assay (Cawthon, 2002). PCR reactions were performed on the iCycler iQ5 2.0 Standard Edition Optical System (Bio-Rad, Hercules, CA), using telomeric primers, primers for the reference control gene (mouse 36B4 single copy gene) and PCR settings as previously described (Liu et al., 2007) (Table S4). For each PCR reaction, a standard curve was made by serial dilutions of known amounts of DNA. The telomere signal was normalized to the signal from the single copy gene to generate a T/S ratio indicative of relative telomere length. Equal amount of DNA (20 ng) was used for each reaction.

Telomere Restriction Fragment Measurement

The telomere restriction fragment (TRF) analysis was performed using a commercial kit (TeloTAGGG Telomere Length Assay, cat no. 12209136001, Roche). DNA was extracted from cells by phenol-chloroform method. A total of 3 μg DNA was digested overnight with MboI endonuclease (NEB) at 37°C and electrophoresed through 1% agarose gels in 0.5 × TBE at 14°C for 16 h at 6 V/cm with an initial pulse time of 1 s and end in 12 s using a CHEF Mapper pulsed field electrophoresis system (Bio-Rad). The gel was blotted and probed

using reagents in the kit. The telomere length is quantified by TeloTool software (Available from https://www.mathworks.com/matlabcentral/fileexchange/44573-telotool-terminal-restriction-fragment-analysis).

Telomere Q-FISH

Telomere length was estimated by telomere Q-FISH as described previously (Herrera et al., 1999; Poon et al., 1999). Telomeres were denatured at 80°C for 3 min and hybridized with FITC- or Cy3-labeled $(CCCTAA)_3$ peptide nucleic acid (PNA) probe at 0.5 μg/ml (F1001, Panagene, Korea). Chromosomes were stained with 0.5 μg/ml DAPI. Fluorescence from chromosomes and telomeres was digitally imaged on a Zeiss microscope with FITC/DAPI or Cy3/DAPI using AxioCam and AxioVision software 4.6. Telomere length shown as telomere fluorescence intensity was integrated using the TFL-TELO program (kindly provided by Peter Lansdorp, Terry Fox Laboratory).

Flow-FISH Analysis of Telomeres

Flow-FISH analysis of telomeres was performed as described previously (Baerlocher and Lansdorp, 2003; Canela et al., 2007). Cells suspension were fixed with 70% alcohol for 10 min at 4°C, and dehydration in 85% alcohol and 100% alcohol. Telomeres were denatured at 80°C for 3 min and hybridized with Cy3-labeled $(CCCTAA)_3$ peptide nucleic acid (PNA) probe at 0.5 μg/ml (F1002, Panagene, Korea). Then cells were shaken and washed three times and FACS analysis performed using a Flow Cytometer (BD Biosciences).

Library Preparation and RNA-Sequencing

mRNA was purified from total RNA using poly-T oligo-attached magnetic beads. Fragmentation was carried out using divalent cations under elevated temperature in NEB Next First Strand Synthesis Reaction Buffer (5x). First strand cDNA was synthesized using random hexamer primer and M-MLV Reverse Transcriptase (RNase H^-). Second strand cDNA synthesis was subsequently performed using DNA Polymerase I and RNase H. Remaining overhangs were converted into blunt ends via exonuclease/polymerase activities. After adenylation of 3′ ends of DNA fragments, NEB Next Adaptors with hairpin loop structure were ligated to prepare for hybridization. To select cDNA fragments of preferentially 150∼200 bp in length, the library fragments were purified with AMPure XP system (Beckman Coulter, Beverly, USA). Then 3 μL USER Enzyme (NEB, USA) was used with size-selected and cDNA adaptor ligated at 37°C for 15 min followed by 5 min at 95°C prior to PCR. PCR was performed with Phusion High-Fidelity DNA polymerase, Universal PCR primers and Index Primer. At last, PCR products were purified using AMPure XP system and library quality assessed on the Agilent Bioanalyzer 2100 system. Cluster of the index-coded samples was performed on a cBot Cluster Generation System using TruSeq PE Cluster Kit (Illumina) according to the manufacturer's instructions. After cluster generation, the library preparations were sequenced on an Illumina Hiseq platform.

For Library preparation of a few cells, 1000 cells per sample were resuspended in PBS with 0.1% BSA and transferred to the bottom of a PCR tube consisting of 3 μL lysis buffer, and cDNA was synthesized in the tube containing mRNA, based on Smart-seq2 protocol (Picelli et al., 2014), and then the libraries were prepared by using TruePrep DNA Library Prep Kit V2 for Illumina® (TD503-02, Vazyme Biotech) according to the manual instruction. Samples were barcoded and multiplex sequenced with a 150-bp paired-end sequencing strategy on an Illumina Hiseq platform.

Bioinformatics Analysis

Clean reads were mapped to the mouse reference mm10 reference genome using Bowtie2 (population) or Hisat2 (a few cells). Reads were assigned and counted to genes using the RSEM. The resulting matrix of read counts was then loaded into RStudio (R version 3.4.2), and DESeq2 were used to identify differentially expressed genes. Functional enrichment (GO annotation or KEGG) of gene sets with different expression patterns was performed using clusterProfiler. The heat-maps were drawn by the function "pheatmap" of R packages and correlation coefficients were calculated by the function "cor" in R. Scatterplots were generated using the "ggplot2" package to graphically reveal genes that differ significantly between two samples. The *p value*s were adjusted using the Benjamin & Hochberg method (Hochberg and Benjamini, 1990). Corrected *P*-value of 0.05 and $\log_2$ (fold change) of 1 were set as the threshold for significantly differential gene expression. Cluster and analysis of XEN-like, 2C, pluripotency, PGCs specific and germ cell genes provided in the heatmap were obtained using RNA-seq data published (Hayashi et al., 2012; Miyauchi et al., 2017; Zhao et al., 2015, 2018). Calculated z score of selected genes was used for heatmap.

Whole-Exome Sequencing

For population cells, paired-end DNA library were prepared according to manufacturer's instructions (Agilent). Genomic DNAs (gDNA) from cell samples were sheared into 180∼280 bp fragments by Covaris S220 sonicator. Ends of gDNA fragments were repaired and 3′ ends were adenylated. Both ends of gDNA fragments were ligated at the 3′ ends with paired-end adaptors (Illumina) with a single 'T' base overhang and purified using AMPure SPRI beads from Agencourt. The adaptor-modified gDNA fragments were enriched by six cycles of PCR using SureSelect Primer and SureSelect ILM Indexing PreCapture PCR Reverse Primer. The concentration and size distribution of the libraries were determined on an Agilent Bioanalyzer DNA 1000 chip. Whole exome capture was carried out using SureSelect Mouse All Exon V1 Agilent 5190-4642. An amount of 0.5 μg prepared gDNA library was hybridized with capture library for 5 min at 95°C followed by 24 h at 65°C. The captured DNA−RNA hybrids were recovered using Dynabeads

MyOne Streptavidin T1. Capture products were eluted from the beads and desalted using QIAGEN MinElute PCR purification columns. The purified capture products were then amplified using the SureSelect ILM Indexing Post Capture Forward PCR Primer and PCR Primer Index (Agilent) for 12 cycles. After DNA quality assessment, captured DNA library were sequenced on Illumina Hiseq 2000 sequencing platform (Illumina) according to manufacturer's instructions for paired-end 150 bp reads (Novogene). Libraries were loaded onto paired-end flow cells at concentrations of 14-15 pM to generate cluster densities of 800,000-900,000 per mm^2 using Illumina cBot and HiSeq paired-end cluster kit.

For GV oocytes, 10 GV oocytes per sample were pre-amplified and amplification based on the method of multiple annealing and looping based amplification cycles (MALBAC) described previously (Zong et al., 2012). Briefly, 30 μL of amplification buffer was added into PCR tubes each containing 10 lysed GV oocytes, followed by incubating the tube at 94°C for 3 min to melt the double-stranded genome DNA into single-stranded form. After melting, the single-stranded genomic DNA molecules were immediately quenched on ice to increase the efficiency of primer binding. Then, 2.5 Units of Bst large fragment (NEB) were added into each PCR tube and the following temperature steps were performed: 10°C for 45 s, 20°C for 45 s, 30°C for 45 s, 40°C for 45 s, 50°C for 45 s, 65°C for 2 min, 94°C for 20 s. The tubes were then quickly quenched on ice. The same polymerase mix was added to provide enzyme for the next round of amplification. The following thermo-cycle was performed before quenching the reactions on ice: 10°C for 45 s, 20°C for 45 s, 30°C for 45 s, 40°C for 45 s, 50°C for 45 s, 65°C for 2 min, 94°C for 20 s, 58°C for 20 s (cycles were repeated 5 times). The product from the MALBAC pre-amplification was further amplified by regular PCR using the following thermal cycle repeated 18 times: 94°C for 20 s, 59°C for 20 s, 65°C for 1 min, and 72°C for 2 min. The amplification products had a size distribution of about 500 bp to 1500 bp, and these products can be used to build DNA library and sequencing using the method mentioned above.

Sequence Alignment and Variant Calling

Variant calling was performed as previously described (Bhutani et al., 2016; Gore et al., 2011). Briefly, paired-end clean reads in FastQ format generated by the Illumina pipeline were aligned to the mouse reference genome mm10 by Burrows-Wheeler Aligner (BWA) to obtain the original mapping results stored in BAM format. SAMtools (http://broadinstitute.github.io/picard/) were used to sort BAM files and generate final BAM files for computation of the sequence coverage and depth. BCF tools were used to call variants, and variants annotation and variant positions were obtained using Variant Annotation software. RefSeq was applied for annotation to determine amino acid alternations. Variants obtained from previous steps were compared against SNPs present in the dbSNP database to discard background SNPs. The consensus sequences in E12.5 PGCs, gPSCs, OG4-ESCs, gPSC4/15-PGCLCs, OG2-GV oocytes and gPSC4/15 GV oocytes samples were then used to compare with progenitor GCs samples to examine candidate novel mutations in coding sequence (CDS).

QUANTIFICATION AND STATISTICAL ANALYSIS

Statistics was analyzed by using the StatView software from SAS Institute Inc. (Cary, NC). Data were analyzed using two-tailed unpaired Student's t test to compare two groups or ANOVA to compare more than two groups and expressed as Mean ± SEM *p value*s less than 0.05 were considered significant ($^{*}P < 0.05$, $^{**}P < 0.01$ or $^{***}P < 0.001$). In addition, data of TFU is expressed as Mean ± SD in the Figures S3F and S3I. The exact values of "n" used are described in the corresponding figure legends. "n" refers to the number of biological replicates and includes either number of mice or replicates of cell studies. FACS data were analyzed by FlowJo, TFU of telomere Q-FISH was quantification by TFL-TELO program, and TRF data were quantification by TeloTool. Graphs were generated using GraphPad Prism or R package ggplot2 or other R packages described in the method details.

DATA AND CODE AVAILABILITY

The accession number for all the RNA sequencing data reported in this paper is NCBI GEO: GSE127833, and all the whole exome sequencing data reported in this paper is NCBI SRA: PRJNA559066.